

1 **Different contact angle distributions for**
2 **heterogeneous ice nucleation in the Community**
3 **Atmospheric Model version 5**

4 Yong Wang^{1,2,3}, Xiaohong Liu^{2,*}, Corinna Hoose⁴, and Bin Wang¹

5 1. *Institute of Atmospheric Physics, Chinese Academy of Sciences, Beijing 100029,*
6 *China*

7 2. *Department of Atmospheric Science, University of Wyoming, Laramie, WY 82071,*
8 *USA*

9 3. *University of Chinese Academy of Sciences, Beijing 100049, China*

10 4. *Karlsruhe Institute of Technology, Institute for Meteorology and Climate*
11 *Research, 76131 Karlsruhe, Germany*

12
13
14 * Corresponding author: xliu6@uwyo.edu
15

16 **Abstract:** In order to investigate the impact of different treatments for the contact
17 angle (α) in heterogeneous ice nucleating properties of natural dust and black carbon
18 (BC) particles, we implement the classical-nucleation-theory-based parameterization
19 of heterogeneous ice nucleation (Hoose et al., 2010) in the Community Atmospheric
20 Model version 5 (CAM5), and then improve it by replacing the original single contact
21 angle model with the probability density function of α (α -PDF) model to better
22 represent the ice nucleation behavior of natural dust found in observations. We re-fit
23 the classical nucleation theory (CNT) to constrain the uncertain parameters (i.e., onset
24 α and activation energy in the single α model; mean contact angle and standard
25 deviation in the α -PDF model) using recent observation datasets for Saharan natural
26 dust and BC (soot). We investigate the impact of time-dependence of droplet freezing
27 on mixed-phase clouds and climate in CAM5, and the roles of natural dust and soot
28 by different nucleation mechanisms. Our results show that when comparing with
29 observations, the potential ice nuclei (IN) calculated by the α -PDF model has a better
30 agreement than that calculated by the single- α model at warm temperatures ($T >$
31 -20°C). More ice crystals can form at low altitudes (with warm temperatures)
32 simulated by the α -PDF model compared with the single- α model in CAM5. All of
33 these can be attributed to different ice nucleation efficiencies among aerosol particles
34 with some particles having smaller contact angles (higher efficiencies) in the α -PDF
35 model. In the sensitivity tests with the α -PDF model, we find that the change of mean
36 contact angle has larger impact on the active fraction at a given temperature than that
37 of standard deviation, even though the change of standard deviation can lead to the

38 transition of freezing behavior. Both the single α and the α -PDF model indicates that
39 the immersion freezing of natural dust plays a more important role in the
40 heterogeneous nucleation than that of soot in mixed-phase clouds. The new
41 parameterizations implemented in CAM5 induce more significant aerosol indirect
42 effect than the default parameterization.

43

44 **1. Introduction**

45

46 Ice microphysical processes in clouds are vital to cloud radiative properties and
47 precipitation formation. They include the primary ice formation, vapor deposition on
48 ice crystals, accretion of cloud droplets by ice crystals, ice aggregation and
49 sedimentation, ice multiplication, sublimation, melting, and convective detrainment of
50 cloud ice (Pruppacher and Klett, 1997; Morrison and Gettelman, 2008). Till now, ice
51 formation mechanisms, especially by heterogeneous ice nucleation, have not been
52 well understood. In mixed-phase clouds with temperatures between 0 and -38°C ,
53 primary ice formation can be via the heterogeneous ice nucleation with the aid of a
54 fraction of aerosol particles called ice nuclei (IN) (DeMott et al., 2010). Various
55 particles can act as IN, which include mineral dust, soot, volcanic ash, and primary
56 biological particles (Hoose and Möhler, 2012; Murray et al., 2012).

57 Mineral dust has been recognized as the most important/atmospherically relevant
58 IN either from the laboratory measurements or field sample studies (Hoose and
59 Möhler, 2012; Murray et al., 2012). Natural mineral dust particles are often internally
60 mixtures of different minerals, quartz and other components (Murray et al., 2012). In

61 order to reduce the complexity encountered in natural mineral dusts, many laboratory
62 studies, on the one hand, have often used commercially available minerals, in
63 particular kaolinite, illite and montmorillonite (Hoose et al., 2008b; Hoose and
64 Möhler, 2012). Other laboratory experiments, on the other hand, used commercially
65 available Arizona Test Dust (ATD) as a surrogate for natural mineral dusts (e.g.,
66 Knopf and Koop, 2006; Marcolli et al., 2007; Kulkarni et al., 2012). ATD can
67 possibly be more ice nucleation active than natural desert dust, either due to its
68 enhanced roughness resulting from the milling or due to its different mineralogical
69 composition (Möhler et al., 2006). Another reason for lower activity of natural dust
70 particles is related to their aging processes in the atmosphere, which may reduce their
71 ice nucleation ability (Sullivan et al., 2010).

72 Heterogeneous ice nucleation occurs via several different mechanisms (Vali, 1985),
73 called nucleation modes (immersion, deposition, condensation, and contact freezing).
74 For immersion freezing, a supercooled cloud droplet containing an ice nucleus
75 nucleates by subsequent cooling at a certain degree of supercooling. Prenni et al.
76 (2007), through airborne measurements of IN number concentration and elemental
77 composition from the U.S. Department of Energy (DOE) Atmospheric Radiation
78 Measurement (ARM) Mixed-Phase Arctic Clouds Experiment (M-PACE) in northern
79 Alaska, found that immersion and/or condensation freezing (instruments can not
80 separate them) may be the dominant freezing mechanism within these clouds. The
81 term “deposition nucleation” describes that the vapor phase directly deposits on a dry

82 ice nucleus and leads to the growth of ice. “Contact freezing” refers to the freezing of
83 a supercooled droplet, which collides with a dry ice nucleus.

84 To represent the heterogeneous IN number and ice nucleation process, several
85 heterogeneous freezing parameterizations have been developed, which can be divided
86 into two groups: singular (or deterministic) hypothesis and stochastic hypothesis. The
87 first, “singular (or deterministic) hypothesis” proposed by Langham and Mason (1958)
88 assumes that the radius of the ice germ forming on the aerosol surface, at a given
89 supercooling, is controlled by surface features, and thermal fluctuations have a
90 negligible influence on ice germ radius. Thus, the freezing of a droplet is only
91 determined by whether the temperature is below the characteristic temperature of the
92 immersed IN in the droplet (Phillips et al., 2008, 2012; DeMott et al., 2010;
93 Niedermeier et al., 2010; Niemand et al., 2012). The second one, the “stochastic
94 hypothesis” proposed by Bigg (1953), holds that heterogeneous ice nucleation is a
95 function of time. During the time an immersed aerosol particle spends at constant
96 environmental temperature, water molecules within supercooled water stay in the
97 thermal fluctuation state of capturing and losing molecules to produce the cluster.
98 This process resembles the structure of ice. When some of these ice germs reach to a
99 size (the critical radius), they become stable and initiate freezing. The presence of a
100 particle surface immersed in a supercooled droplet is helpful for ice formatting by
101 reducing the number of water molecules that are required to reach the stable cluster
102 radius by letting the germ form on it as a spherical cap. The rate of heterogeneous
103 nucleation per aerosol particle and per time is referred to as the nucleation rate (J_{het}).

104 This stochastic approach can be described by the classical nucleation theory (CNT)
105 (Chen et al., 2008; Hoose et al., 2010; Niedermeier et al., 2011; Welti et al., 2012).

106 In CNT, J_{het} is proportional to the aerosol surface area and is the function of contact
107 angle (α), which is the angle where ice germ/liquid or ice germ/vapor interface meets
108 the aerosol surface, and can be understood as the surrogate of the nucleation ability of
109 aerosol particles. The particle with the smaller contact angle (α) has higher ice
110 nucleating efficiency. The contact angle is often derived from the fitting to the
111 laboratory data, as done in Marcolli et al. (2007) for ATD, in Lüönd et al. (2010) for
112 kaolinite, and in Wheeler and Bertram (2012) for kaolinite and illite. As noted in these
113 studies, assuming that each particle has the same fixed contact angle often does not fit
114 to the observation data well, especially when the observed ice nucleating fraction
115 increases slowly with the increase of time (Welti et al., 2012). These authors
116 suggested to use a probability density function of contact angles (α -PDF) instead of
117 single values to better fit to the observed frozen fraction as a function of temperature
118 (for immersion/condensation nucleation) or supersaturation (for deposition
119 nucleation). In this α -PDF model, contact angles are distributed to every particle,
120 which means that each particle has one value of the contact angle and that the
121 particles with low contact angles are rapidly depleted when the temperature is held
122 constant, thus leading to a slow-down of the freezing of the sample. The α -PDF
123 model can be interpreted as an “intermediate” approach based on CNT between the
124 two extremes of stochastic and singular hypotheses (Niedermeier et al., 2010).

125 Several heterogeneous ice nucleation parameterizations which are based on
126 laboratory studies or in-situ measurements have been implemented in global climate
127 models (GCMs). Liu et al. (2007) implemented Meyers et al. (1992) in CAM3 and in
128 CAM5 (Gettelman et al., 2010) for the immersion/condensation/deposition
129 mechanisms. Xie et al. (2013) evaluated the DeMott et al. (2010) parameterization in
130 CAM5, in comparison with Meyers et al. (1992). Lohmann and Diehl (2006)
131 implemented the Diehl and Wurzler (2004) parameterization in the global climate
132 model of the Max Planck Institute for Meteorology (ECHAM5) for the immersion
133 freezing of cloud droplets. Hoose et al. (2010) implemented the CNT in CAM3-Oslo
134 for the immersion, deposition and contact freezing of dust, soot, and biological
135 aerosols. In their paper, they suggest that assuming stochastic ice nucleation with all
136 particles having the same fixed single contact angle can not fit some observations very
137 well. Immersion freezing and deposition nucleation by dust in Hoose et al. (2010) are
138 fitted to the observation data obtained specifically for montmorillonite (Pitter and
139 Pruppacher, 1973) and illite (Zimmermann et al., 2008) respectively. Thus their
140 results may not reflect the ice nucleation behavior by natural dust particles, which are
141 mixtures of complex mineral components.

142 In this study, we implement the single- α model (Hoose et al. 2010) in CAM5 to
143 represent the heterogeneous ice nucleation of natural dust and BC in mixed-phase
144 clouds. The single- α model is further improved by the α -PDF model to correct the
145 time-dependent behavior of droplet freezing. To better represent the ice nucleation of
146 natural dust found in ambient observations, we use recent observation data on Saharan

147 dust to constrain the parameters used in the CNT parameterization. The model
148 description is presented in section 2. Section 3 describes the CNT parameterizations,
149 with the resulting fitting parameters. In section 4, the model experiments and results
150 are presented. Uncertainties and implications are discussed in section 5.

151

152 **2. CAM5**

153 CAM5 includes a two-moment stratiform cloud microphysics scheme (Morrison
154 and Gettelman 2008 (MG08); Gettelman et al., 2008, 2010). This scheme predicts
155 number concentrations and mass mixing ratios of cloud droplets and ice crystals,
156 while the number concentrations and mass mixing ratios of snow and rain are
157 diagnosed. MG08 treats the microphysical conversions among cloud liquid droplets,
158 ice crystals, rain and snow. As for cloud droplet activation, it follows the
159 Abdul-Razzak and Ghan (2000) parameterization. MG08 was further updated in
160 CAM5 (Gettelman et al., 2010) to implement the Liu et al (2007) scheme for ice
161 crystal nucleation in mixed-phase and cirrus clouds. In mixed-phase clouds, Meyers et
162 al. (1992) is used for deposition, immersion, and condensation freezing of cloud
163 droplets, which, however, does not provide a link of ice nuclei (IN) number
164 concentration to aerosol properties. In addition, the Young (1974) scheme is used for
165 the contact freezing of cloud droplets by the coarse mode dust.

166 CAM5 includes a modal aerosol module (MAM) to represent aerosol processes
167 and properties in the atmosphere (Liu et al., 2012a). It predicts aerosol number
168 concentrations and mass mixing ratios of multiple aerosol species in three aerosol

169 modes: Aitken, accumulation and coarse mode. MAM treats major aerosol species
170 including mineral dust, BC, sea salt, sulfate, and primary and secondary organic
171 aerosols. These aerosol species are internally mixed within a single mode, but
172 externally mixed between different modes. Aerosol species in cloud-borne states are
173 also explicitly treated, but not predicted in the model.

174 The deep convection scheme in CAM5 follows Zhang and McFarlane (1995) but
175 with the dilute Convective Available Potential Energy (CAPE) modification described
176 in Neale et al. (2008). The shallow convection scheme is from Park and Bretherton
177 (2009). The stratus-radiation-turbulence interactions in CAM5 are explicitly simulated
178 by the moist turbulence scheme (Bretherton and Park, 2009). The radiative transfer
179 calculations for aerosol and cloud radiative effects are based on the Rapid Radiative
180 Transfer Model for GCMs (RRTMG) (Iacono et al., 2008).

181

182 **3. New Heterogeneous Ice Nucleation Parameterization in CAM5**

183 **3.1. Single Contact Angle (α) Model**

184 In the CNT, ice nucleation is treated as a stochastic process (Pruppacher and Klett,
185 1997). An energy barrier has to be passed to capture more molecules to small
186 agglomerates of ice (subcritical germs) on the surface of ice nucleus, until a critical
187 germ size is reached. Following the notation in Hoose et al. (2010), both deposition
188 and immersion freezing can be treated in the same general form based on the CNT.
189 Following the suggestion of Chen et al. (2008), we calculate the contact freezing with

190 the critical germ radius of immersion freezing and the homogeneous energy of germ
191 formation of deposition freezing, according to “Cooper’s hypothesis” (Cooper, 1974).

192 We modify the original expression used in Hoose et al. (2010) about J_{het} , the rate of
193 heterogeneous nucleation per aerosol particle and per second, with the form factor (f)
194 raised to the $-1/2$ power instead of $1/2$ (see equation 1), due to the unphysical behavior
195 of the original expression which implies that $J_{het} \rightarrow 0$ when $f \rightarrow 0$ (i.e., the ice
196 nucleation rate will become smaller on more easily wettable materials) (Määttä et al.
197 al., 2005; Barahona, 2012).

$$J_{het} = \frac{A' r_N^2}{\sqrt{f}} \exp\left(\frac{-\Delta g^\# - f \Delta g_g^o}{kT}\right) \quad (1)$$

198 where A' is a prefactor, r_N is the aerosol particle radius, f is a form factor
199 containing information about the aerosol’s ice nucleation ability, $\Delta g^\#$ is the
200 activation energy, Δg_g^o is the homogeneous energy of germ formation, k is the
201 Boltzmann constant, and T is the temperature in K.

202 The second modification is about f itself. Due to the uncertainty of assuming a
203 spherical substrate (or any other simple geometry) (Barahona, 2012), and the
204 difference between a flat surface and a spherical surface can be ignored when the
205 diameter of particle is larger than 100 nm, we calculate the compatibility parameter f
206 with a flat surface instead of the convex surface. Thus f has the form as (Pruppacher
207 and Klett, 1997)

$$f = \frac{1}{4}(2 + m)(1 - m)^2 \quad (2)$$

208 where $m \equiv \cos \alpha$, α is the contact angle.

209 Except for the above changes, detailed descriptions on the formulation of CNT for
210 the immersion, deposition and contact freezing can be found in Hoose et al. (2010).
211 We note that Hoose et al. (2010) used the activation fraction of aerosols, which is
212 diagnosed from the droplet activation parameterization, to partition dust and soot
213 number concentrations in each grid into the interstitial portion for the deposition and
214 contact freezing and into the cloud borne portion for the immersion freezing. However,
215 in CAM5 we directly use the interstitial and cloud borne dust and soot number
216 concentrations in the ice nucleation calculation, since CAM5 explicitly treats these
217 two states of aerosols.

218

219 **3.2. α -PDF Model**

220 We consider the α -PDF model for the immersion freezing by natural dust to replace
221 the single- α model in Hoose et al. (2010). In the α -PDF model, we can take the
222 heterogeneity of individual particles in the aerosol population into account. The
223 particle surface is still uniform in the ice nucleation property for each particle but
224 differs within an ensemble of particle population by a distribution of different contact
225 angles, which are assumed to follow a log-normal probability density function
226 (Marcolli et al., 2007; Lüönd et al., 2010)

227 The log-normal probability density function which represents the occurrence
228 probability of one contact angle for one particle is given by

$$p(\alpha) = \frac{1}{\alpha\sigma\sqrt{2\pi}} \exp\left(-\frac{(\ln(\alpha) - \ln(\mu))^2}{2\sigma^2}\right) \quad (3)$$

229 Where μ is the mean contact angle and σ is the standard deviation.

230 The frozen fraction for a given temperature can then be calculated as

$$f_{act,\alpha-pdf} = 1 - \int_0^{\pi} p(\alpha) \cdot \exp(-J_{imm}(T, \alpha)\Delta t) d\alpha \quad (4)$$

231 Here J_{imm} is the immersion nucleation rate for one particle with one certain contact
232 angle, and Δt is the model time step. It should be mentioned that in the global climate
233 model, the different time dependences of the frozen fraction in the single- α model and
234 the α -PDF model are only treated within one time step. In the current CAM5 model,
235 because of the added complexity and the computational demands, aerosol scavenging
236 due to droplet freezing is not taken into account. It means only if the active fractions
237 are large enough in the last time step, in the following time step additional (and
238 unphysical) ice nucleation would occur with both contact angle distributions if
239 temperature is constant. Especially for the α -PDF model, as particles with small
240 contact angles are not scavenged in each time step, these small contact angles can not
241 be tracked with time in the model to adjust the distribution of contact angle (adding
242 even more complexity). However, since we directly use predicted cloud borne dust
243 and BC, during each model time step (30 minutes) cloud borne aerosols will be
244 updated, which means that fresh particles as cloud condensation nuclei (CCN) will be
245 nucleated into cloud droplets. As the new parameterizations implemented in this study
246 predict the active fractions due to droplet freezing in one model time step of 30 min
247 are much smaller than 100% (see e.g. Figure 2), these newly-formed cloud droplets
248 are sufficient to make up those depleted amount of cloud droplets (i.e., Δt in Eq. (4)
249 may be also thought as time scale to replenish IN population in a grid point).
250 Moreover, after the Wegener-Bergeron-Findeisen process sets in, further ice

251 nucleation will be suppressed. Overall, In this case we actually benefit from the long
 252 time step because the clouds and the environmental conditions change significantly
 253 from time step to time step, such that starting from fresh is not a bad assumption. In
 254 particular, entrainment of new IN, temperature changes and the shutdown of ice
 255 nucleation through the Bergeron process are thought to be important. Therefore, no
 256 aerosol scavenging due to droplet freezing and assuming a constant distribution of
 257 contact angles in the α -PDF model among time steps only causes the new
 258 parameterizations to have a small artifact. Another point is that new parameterizations
 259 in the CAM5 model reduce nucleated ice crystals compared to the default Meyers et
 260 al. scheme (see Table 4), which means that the depletion of cloud-borne aerosols has a
 261 smaller effect on model results than the default scheme.

262

263 **3.3. Fitting Parameters for Natural Dust and Soot**

264 Fitting parameters in the CNT such as the single contact angle (α) and activation
 265 energy ($\Delta g^\#$) in the single- α model can be derived by minimizing the root mean square
 266 error (RMSE) of frozen fractions between observation data and model results. Thus
 267 the RMSE is calculated as:

$$RMSE = \sqrt{\frac{1}{N} \sum_1^N [F_{ice} - F_{ice}^{mod}]^2} \quad (5)$$

268 where F_{ice} is the observed frozen fraction, F_{ice}^{mod} is the frozen fraction calculated
 269 from the single- α model, and N is total number of observation data points.

270 The formula to derive uncertain parameters in the α -PDF approach is the same as
271 Eq. (5) except that we calculate F_{ice}^{mod} from the α -PDF model. In order to calculate
272 F_{ice}^{mod} , its integral form of Eq. (4) was discretized into 2000 bins, and then the PDF
273 distribution parameters, standard deviation (σ) and mean contact angle (μ) were
274 iterated to find the best fit following Eq. (5).

275 The resulting fitting parameters for the immersion and deposition freezing based
276 on the single- α model are listed in Table 1. Observation data for the immersion
277 freezing of dust is obtained from the Colorado State University CFDC-HIAPER
278 version I (CSU CFDC-IH) experiment, which is selected for the relative humidity
279 with respect to water (RH_w) at 106% (CSU106) (DeMott et al., 2011), and data for the
280 deposition freezing on dust is from the Koehler et al. (2010)'s laboratory study. Both
281 of the two studies used samples for Saharan dust, which generally contain quartz,
282 feldspars and clay minerals in different compositions (Linke et al., 2006). The
283 immersion and deposition by soot are still based on the measurements (DeMott, 1990;
284 Möhler et al., 2005) used in Hoose et al. (2010). However due to the modification of
285 expressions of J_{het} and f in section 3.1, we refit to these data again. In the case of
286 deposition freezing in Table 1, $\Delta g^\#$ is negative and the reason is as follows. $\Delta g^\#$
287 (activation energy) is the energy of desorption per molecule, which stands for the
288 surface with the outward flux of desorbed molecules. Instead, J_{het} specifies the flux
289 of water molecules to the germs. Actually in J_{het} for the deposition freezing, there
290 should be no a negative sign before $\Delta g^\#$ (see Eq. 9-8b in Pruppacher and Klett,
291 1997). However, in order to use the unified formula for both immersion and

292 deposition freezing (Eq. 1), a negative sign is added before $\Delta g^\#$ (as in Chen et al.,
293 2008). Thus the fit result for the activation energy in the case of deposition freezing is
294 negative to offset this negative sign.

295 For the α -PDF model, in the formulation by Chen et al. (2008), the activation
296 energy for the transfer of a water molecule across the water-ice boundary is aerosol,
297 nucleation mode and temperature dependent and thus should from a theoretical
298 standpoint be independent on the contact angle (Zobrist et al., 2007; Hoose et al.,
299 2010), we use the same value for the activation energy as that in the single- α model.
300 The resulting fit parameters from different experiments are listed in Table 2. For the
301 comparison, fit parameters with the single- α model, including CSU106 listed in Table
302 1, are also given. The experiments were performed over a wide temperature range for
303 Saharan dust sampled in the 2007 International Workshop on Comparing Ice
304 Nucleation Measuring Systems ICIS-2007 (DeMott et al., 2011). These include two
305 experiments of CSU CFDC-IH with 106% and 108% RH_w (CSU106 and CSU108,
306 respectively), and three experiments conducted with the Zurich Ice Nuclei Chamber
307 (ZINC) at RH_w of 106%, 108% and 110% (ZINC106, ZINC108, and ZINC110,
308 respectively). It can be seen that the RMSEs with the single- α model in all five
309 experiments are larger than those with the α -PDF model. The reason about this result
310 can be seen from the Figure 1, which shows the observation data from CSU106 and
311 ZINC106, and their fits with the single- α model and the α -PDF model. The α -PDF
312 model reproduces the slow decrease of active fraction with the increase of
313 temperature and makes a better agreement with observation data points at warm

314 temperatures ($T > -20^{\circ}\text{C}$) while the single- α model leads to a steep decrease of active
315 fraction with the increase of temperature and thus results in large errors at warm
316 temperatures. Therefore, larger RMSEs with the single- α model are mainly from its
317 fit at warm temperatures (CSU106 for $T=-18.5^{\circ}\text{C}$ and ZINC106 for $T=-27.7^{\circ}\text{C}$). At
318 warmer temperatures between -10° and -15°C , there are no CFDC observation data to
319 constrain the parameterizations because CFDC cannot provide observation data at
320 warm temperatures ($> -15^{\circ}\text{C}$). However, Niemand et al. (2012) reported the Aerosol
321 Interactions and Dynamics in the Atmosphere (AIDA) cloud chamber measurement of
322 natural dust at temperatures of -13 and -16°C with active fractions of 10^{-4} and 10^{-5} ,
323 which agree with our fitted active fractions from the α -PDF model. As Saharan
324 natural dust is reported in recent CFDC observations that it has onset temperatures
325 ranging from about -10° to -15°C , which is consistent with laboratory observations of
326 various types of surrogate dust (Phillips et al., 2012). Therefore, we apply a cut off of
327 0 for the active fractions at temperatures larger than -10°C for two contact angle
328 distributions.

329

330 **3.4. Sensitivity Tests of Time Dependence**

331 We perform sensitivity tests to check whether it is appropriate to use a
332 classical-theory-based parameterization with a crude time step of 30 minutes in the
333 CAM5 model. Figure 2 shows the active fraction with different contact angle
334 distributions as a function of integration time at different temperatures. It can be seen
335 that at $T = 263\text{ K}$ the active fractions in all contact angle distributions are almost

336 constant with time, indicating very weak dependence of the active fraction on time at
 337 warm temperature (the active fractions in the α -PDF models with $\sigma = 0.01$ and $\sigma =$
 338 0.08 are about 0.499×10^{-5} and 0.516×10^{-5} respectively, so these two lines are
 339 overlapped). At $T = 253$ K and $T = 243$ K, the active fractions in the single- α model
 340 and the α -PDF models with $\sigma = 0.01$ and 0.08 increase with time (the α -PDF model
 341 with $\sigma = 0.01$ is very similar as the single- α model), but the active fraction in the
 342 α -PDF model with $\sigma = 0.08$ is a little insensitive to time than that in the single- α
 343 model. With increasing standard deviation in the α -PDF model, the active fractions
 344 become weaker dependent on time, especially for the weakest time dependence with σ
 345 $= 1.0$. As the single- α model can be thought as the special α -PDF model with $\sigma = 0$,
 346 and increasing the standard deviation reduces the time dependence, we can conclude
 347 the single- α model has stronger time dependence than the α -PDF model, which is
 348 consistent with Welte et al. (2012). Although the single- α model has stronger time
 349 dependence, if we use the following diagnostics, originally developed by Ervens and
 350 Feingold (2013), to determine the sensitivity of the active fraction to time in detail, we
 351 will find the active fraction in the single- α model is still only weakly dependent on
 352 time.

$$S(X) = \frac{\partial P}{\partial \ln X} \quad (6)$$

353 where P is the active fraction, X can be any of parameters from temperature, particle
 354 size, contact angle or time. At $T = 253$ K, from $t = 10$ s ($P = 0.00011$) to $t = 1800$ s ($P =$
 355 0.02), $S(X)$ is 0.0038 . At $T = 243$ K, from $t = 10$ s ($P = 0.013$) to $t = 1800$ s ($P = 0.9044$),

356 $S(X)$ is 0.172. The very small values of $S(X)$, which are consistent with the values in
357 Ervens and Feingold (2013), indicate that the active fraction in the single- α model is
358 the least sensitive to time. Ervens and Feingold (2013) performed many sensitivity
359 tests to investigate relative importance of temperature, particle size, contact angle and
360 time for classical nucleation theory. They used Eq. (6) to explore the sensitivity of the
361 active fraction to the above four parameters. From Figure 1(a) to Figure 1(d) of their
362 paper, they found from comparison of $S(X)$ that among the four parameters P is the
363 least sensitive to time. Ervens and Feingold (2013) concluded that a change in T
364 (temperature) of ~ 1 K has a similar impact on P (the active fraction) as θ (contact
365 angle) changes of $\Delta\theta = 2^\circ$ whereas a similar change is only caused by an increase in
366 D_{IN} (particle diameter) by one order of magnitude or in t (time) by three orders of
367 magnitude. They hence suggested that it seems feasible to develop more physically
368 (CNT) based relationships instead of those empirically based relationships in
369 large-scale models. Therefore, the overestimate of the frozen fraction due to a crude
370 time step of 30 min is negligible compared to the uncertainties in temperature and
371 mean contact angle.

372

373 **4. Results**

374 A control experiment (CTL) with the default freezing parameterization in CAM5
375 (Meyers et al., 1992), an experiment based on the CNT in Hoose et al. (2010)
376 (single- α), an experiment with the new α -PDF model as described above, and several

377 sensitivity experiments with the α -PDF model have been carried out (see Table 3).
378 The sensitivity experiments are designed to explore the sensitivities of model
379 simulations to the mean contact angle and standard deviation in the α -PDF model.
380 The mean contact angle is changed by $\pm 15^\circ$ (in order to include 61° , which is the fit
381 result from the ZINC measurements), and standard deviation increased by 4 and 8
382 times in these sensitivity experiments.

383 All these simulations are run for 6 years with the model configuration of $1.9^\circ \times 2.5^\circ$
384 and 30 levels, using prescribed sea surface temperatures (SST) and sea ice extent. The
385 aerosol input uses the online aerosol model, MAM3. The last 5-year results are used
386 in the analysis.

387

388 **4.1. Particle Number Concentrations**

389 The zonal and annual mean number concentrations of interstitial, cloud borne and
390 total (interstitial plus cloud borne) mineral dust and soot particles are shown in Figure
391 3. As is shown in Figure 3, the magnitudes of interstitial dust and soot number
392 concentrations are about one order of magnitude larger than those of cloud borne ones.
393 In cloud borne aerosols, there are more dust particles than soot particles, which is an
394 important point to explain the dominant role of dust in heterogeneous freezing
395 compared to soot. The maximum number concentration of interstitial soot, internally
396 mixed in the accumulation mode, is near the surface in the Northern Hemisphere
397 (NH), exceeding 50 cm^{-3} in the zonal mean. Interstitial mineral dust particles in the
398 accumulation and coarse mode, reach $10\text{-}50 \text{ cm}^{-3}$ in the sub-tropics and at the surface

399 of NH ($\sim 30^\circ\text{N}$). Interstitial mineral dust and soot are uplifted from their source
400 regions to the middle and upper troposphere and transported to the Arctic in the upper
401 troposphere (Liu et al., 2012b). The total number concentrations of these two species
402 are mainly from their interstitial particles. As noted above, cloud borne aerosols are
403 used as an input for the immersion freezing, while interstitial aerosols (only the
404 uncoated portion showed in Figure 4) are used as an input for deposition and contact
405 freezing (see next paragraph for definitions of coated and uncoated portion).
406 Compared to Hoose et al. (2010), the total number concentration of soot is one order
407 of magnitude lower in CAM5, which can be attributed to the different size
408 distributions used for soot in two models (CAM5 and CAM3-Oslo). In the
409 CAM3-Oslo model, soot is emitted into the nucleation (initial diameter: $0.024\ \mu\text{m}$),
410 the Aitken (initial diameter: $0.08\ \mu\text{m}$) and accumulation (initial diameter: $0.2\ \mu\text{m}$)
411 modes (Seland et al, 2008). Its number concentration is dominated by uncoated
412 nucleation and Aitken mode particles, which contribute to the higher number
413 concentration, while in CAM5 soot is emitted in the accumulation mode with a larger
414 emission size ($0.08\ \mu\text{m}$ in diameter). Dust number concentrations in CAM5 are
415 mainly from the accumulation mode with the diameter range of $0.1\text{-}1.0\ \mu\text{m}$, while
416 coarse mode number concentration is one order of magnitude lower (Liu et al., 2012a).
417 A similar ratio between accumulation and coarse mode dust is also found in
418 CAM3-Oslo.

419 The interstitial mineral dust and soot particles are further divided into two
420 categories: coated and uncoated particles. The number concentrations of them are

421 derived from the coated fraction f_{coated} , which is calculated by distributing the soluble
422 mass (sulfate and organic) over the soot and dust cores in the internally mixed modes,
423 requiring a minimum coverage of one monolayer. Suppression of heterogeneous ice
424 nucleation is dependent on coating thickness or the fractional soluble mass coverage.
425 Generally we assume that if a potential IN is covered by more than one monolayer, its
426 heterogeneous nucleation behavior in the deposition and contact modes will be
427 suppressed completely due to a shift to the higher onset relative humidity with respect
428 to ice, RH_i , and to the colder onset temperature (Hoose et al., 2010; Möhler et al.,
429 2008). Therefore, only those uncoated particles will participate in ice nucleation. The
430 number concentrations of coated and uncoated interstitial aerosol particles are shown
431 in Figure 4. It can be seen that the uncoated dust number concentration is several
432 orders of magnitude lower than that of coated dust particles, with the criteria of one
433 monolayer coating by soluble aerosol species. Compared to dust, nearly all the soot
434 particles are coated (the concentration of the uncoated soot particles is smaller than
435 10^{-6} cm^{-3}). This is because soot cores have the smaller sizes than dust cores and soot is
436 directly emitted into the accumulation mode in MAM3. If soot is directly emitted into
437 the primary carbon mode (e.g., MAM4 or MAM7), which is the insoluble mode, there
438 should be much more uncoated soot particles, especially with slow aging of the
439 primary carbon mode (not shown in this paper). However, as compared to dust, soot is
440 a much less efficient IN and immersion freezing is the dominant process (see section
441 4.2), it won't have large effects on the total nucleated ice number concentrations even
442 using MAM4 or MAM7.

443

444 **4.2. Ice Nucleation Rates**

445 The zonal and annual mean rates of immersion, deposition, and contact freezing
446 ($\Delta N_i/\Delta t$, here ΔN_i is the ice crystal number concentration change only predicted from
447 the immersion, deposition and contact freezing respectively over one model time step
448 Δt (30 min); note that it is different from J_{het}) by dust and soot in the PDF simulation
449 are shown in Figure 5. It can be seen that the immersion freezing by dust is the
450 dominant ice nucleation mechanism, which is consistent with Hoose et al. (2010),
451 followed by soot immersion, dust deposition, and dust contact freezing. Recent
452 observations (de Boer et al., 2011) also indicated that immersion freezing may be the
453 dominant freezing mechanism in mixed-phase clouds, compared to other freezing
454 modes (deposition freezing and contact freezing). This was concluded from the
455 observation that liquid droplets occurred prior to the ice formation in mixed-phase
456 clouds, which was also detected by Ansmann et al. (2008). A recent laboratory study
457 by Bunker et al. (2012) found that hundreds of collisions of mineral dust particles
458 with a supercooled droplet are needed to initiate the contact freezing. Thus the contact
459 freezing might not be a dominant ice formation pathway in mixed-phase clouds. The
460 other two nucleation modes by soot (i.e., soot deposition and soot contact) are nearly
461 negligible, because the number concentration of uncoated interstitial soot particles is
462 very small (see Figure 4). In general, the ice nucleation rates peak over the regions
463 where dust and soot particles are emitted. It should be noted here that freezing rates
464 appear larger than 0 at $T > 0$ °C and $T < -37$ °C is due to the zonal and annual

465 averaging. The vertically integrated and globally averaged nucleation rates in the PDF
466 simulation are shown in Figure 6. The relative roles of all these rates in mixed-phase
467 clouds can be seen more clearly. The freezing rates by dust are similar to those of
468 Hoose et al. (2010). However, the freezing rates by soot are much smaller because of
469 the large differences in the simulated soot number concentrations between two models
470 (CAM5 and CAM-Oslo) as well as the internal mixture of soot in the accumulation
471 mode assumed in CAM5 (section 4.1), which leads to smaller ice nucleation rates in
472 CAM5. In CAM-Oslo, a larger fraction of the soot particles are uncoated and can thus
473 contribute to deposition and contact nucleation, which we do not consider realistic, in
474 particular as these two processes are not observed at warm subzero temperatures in
475 laboratory experiments.

476 For the comparison, the immersion freezing rates by dust simulated by the single- α
477 (CNT) and α -PDF (PDF) models are shown in Figure 7. We can see that compared to
478 the single- α model, the major increases of the freezing rates in the α -PDF model
479 locate at low altitudes (with warm temperatures), which is attributed to the PDF
480 distribution of contact angles in the α -PDF model. It means that particles with smaller
481 contact angles in the α -PDF model can nucleate at warm temperatures where the
482 particles with the same contact angles in the single- α model can't nucleate.

483

484 **4.3. Occurrence Frequency of Ice Nucleation Modes**

485 In order to count the different ice nucleation events, we follow the same method as
486 that in Liu et al. (2012b), which counts the homogeneous ice nucleation and

487 heterogeneous ice nucleation events in cirrus clouds when there are new nucleated ice
488 number concentrations from these two ice nucleation modes respectively. Therefore,
489 in this study, only when the freezing rate ($\Delta N_i/\Delta t$) from one ice nucleation mode is
490 larger than 0, then we count this ice nucleation event. The occurrence frequency of
491 immersion freezing, deposition nucleation and contact nucleation as a function of
492 temperature sampled every 3 hours from the PDF simulation and the frequency of
493 immersion freezing from the CNT simulation are shown in Figure 8. All the data in
494 each temperature bin (2 K) are shown with the whiskers indicating the 5th and 95th
495 percentiles and with the boxes indicating the 25th and 75th percentiles. The
496 occurrence frequencies for a period of 5 years (hourly data) are output between -90°S
497 to 90°N and from 1000 hPa to 500 hPa. It is obvious to see that the frequency of
498 immersion freezing is higher than contact nucleation and deposition nucleation, At
499 warm temperatures ($T > 257\text{ K}$), the frequency of deposition nucleation decreases
500 rapidly with the increase of temperature, resulting in one order of magnitude smaller
501 than contact nucleation. The frequency of immersion freezing in the PDF simulation
502 at $T > 261\text{ K}$ is higher than that in the CNT simulation.

503 Figure 9 shows the zonal and annual mean frequency distribution of immersion
504 freezing, deposition nucleation and contact nucleation. The pattern of immersion
505 freezing is different from the two other modes. There are two maximum centers
506 located in the polar regions. The deposition and contact nucleation peak over the
507 source regions at 30°N - 60°N and 20°S - 40°S . It is because dust and soot near the
508 source regions are uncoated, leading to occurrence of the deposition and contact

509 nucleation. When these particles age and are coated in the process of uplifting and
510 transporting to polar regions, the deposition and contact nucleation become even less
511 important and conversely immersion freezing dominates. The frequency of immersion
512 freezing after introducing the α -PDF model (PDF) compared to the single- α model
513 (CNT) is increased a little at low altitudes (with warm temperatures).

514

515 **4.4. Sensitivity Tests with the α -PDF Model**

516 Figure 10 shows the effects of changes of the uncertain parameters in the α -PDF
517 model on active fraction with temperature. Figure 10(a) shows the impact of mean
518 contact angle. It's obvious that with the decrease of the mean contact angle, the active
519 fraction increases, making the curve shift upwards. However, the temperature range in
520 which ice fraction rapidly increases doesn't become broader, indicating that changes
521 of the mean contact angle do not change much the slope of variations of active
522 fraction with temperature. Instead in Figure 10(b), the temperature dependence of the
523 active fraction changes with the change of the standard deviation. With the increase of
524 standard deviation, a broader distribution of contact angles will be allocated to aerosol
525 particles. Since the different contact angle on each particle results in the different
526 freezing temperature of each particle, the temperature range in which droplets freeze
527 becomes broader. For example, for $\sigma = 0.01$, droplets freeze within a narrow
528 temperature interval of about 10 °C, while for $\sigma = 0.08$, freezing occurs over a
529 temperature range of about 18 °C. The change of the activated fraction with
530 temperature (Figure 10(b)) becomes smoother with increase of the standard deviation,

531 which indicates the “recovery” of the singular behavior (Niedermeier et al., 2011,
532 2014; Welti et al., 2012) and weakening of the time dependence of the stochastic
533 behavior (see Figure 2 for the change of the time dependence with increase of the
534 standard deviation). Although the magnitude of changes of active fraction due to the
535 change of the standard deviation is much smaller than that due to the mean contact
536 angle at a given temperature, increasing the standard deviation results in the transition
537 of the freezing behavior, from the stochastic behavior to the singular behavior
538 (Niedermeier et al., 2011, 2013). Some variances of cloud properties with the changes
539 of these uncertain parameters in the α -PDF model will be shown in section 4.6.

540

541 **4.5. Comparison of IN Concentrations with Observations**

542 Currently the mostly used instrument for detecting IN concentrations in the
543 atmosphere is the continuous-flow diffusion chamber (CFDC) (Rogers et al., 2001),
544 which allows interstitial aerosol particles to enter through an inlet and to expose a
545 specific temperature and/or humidity in the chamber. Then the number concentration
546 of ice crystals nucleated in the chamber after a residence time of 5-20 s is counted.
547 We calculate modeled IN concentrations and compare them with CFDC observations.
548 The calculation uses modeled interstitial aerosol concentrations which are sampled at
549 the same locations and pressures as observations and with the same processing
550 temperatures as operated in the CFDC. In the same way, the relative humidity is
551 assumed to be equal to the processing conditions in the instrument. It is assumed in
552 our calculations that 100% of the relative humidity with respect to water (RH_w) is

553 used for the immersion freezing, and 98% RH_w for the deposition freezing. Thus
554 immersion/condensation and deposition nucleation modes are taken into account,
555 which is consistent with the observed dominant ice nucleation modes in the CFDC.
556 The reason that the contact nucleation mode is not considered is that the residence
557 time in CFDC is short and thus its technique can not directly assess whether aerosols
558 particles are active as contact freezing nuclei (DeMott et al., 2010).

559 Both the single- α and α -PDF models are time dependent, and CFDC has a
560 residence time of approximate 10 s, so we define the modeled IN number
561 concentration (hereafter termed “model IN(10s)”) as a 10 s integral over the freezing
562 rate ($\Delta N_i/\Delta t$) for a direct comparability to the observations, following Hoose et al.
563 (2010). Figure 11 shows the model IN(10s) concentrations in two simulations (CNT
564 and PDF), which are diagnosed based on interstitial aerosol concentrations from the
565 simulations at the measurement locations and are diagnosed at the same pressure level
566 as field observations. The magnitude of model IN(10s) concentrations simulated by
567 CNT and PDF are similar as observations except for Barrow, Alaska (some data
568 points which are clearly below the acceptable minimum detection limit of CFDC are
569 removed). At warmer temperatures ($T > -20^\circ\text{C}$) model IN(10s) concentrations
570 simulated by the PDF simulation at Colorado region from winter icing in storms
571 project in 1994 (WISP94) in February and at Storm Peak in April/May agree with
572 observations better than those by CNT in which the simulated IN(10s) concentrations
573 are several orders of magnitude smaller than observations. The modeled weak
574 temperature dependence at $T > -20^\circ\text{C}$ in Colorado region in the PDF simulation is

575 confirmed by observations, where there is an indication for trend to be flatter (the
576 observation data in Lüönd et al. (2010) also has this trend at warm temperatures).
577 Conversely, when the temperature is warmer than -20°C , the IN(10s) concentrations
578 simulated by the CNT simulation reduce rapidly, resulting in several orders of
579 magnitude discrepancy with observations (see Figure 11(a) and Figure 11(c)). The
580 temperature variation of model IN(10s) concentrations in the CNT and PDF
581 simulations become flat at $T < -25^{\circ}\text{C}$ at Storm Peak, which is consistent with the
582 observations. The model IN(10s) concentrations at Barrow, Alaska in the CNT and
583 PDF simulations are both one or two orders of magnitude smaller than observations.
584 Due to good agreement of IN(10s) concentrations with other observations (see Figure
585 11(a)-(c)) and confirmed relationship between IN concentrations and aerosol number
586 concentrations with diameter larger than $0.5\ \mu\text{m}$ for all gridpoints (see Figure 12 in
587 detail), we may derive that the simulated aerosol number concentrations with diameter
588 larger than $0.5\ \mu\text{m}$ in these locations (i.e., Figure. 11(a)-(c)) should be in agreement
589 with observations and the large underestimates of IN(10s) concentrations in Barrow,
590 Alaska is the fact that the simulated number concentrations of aerosol particles (e.g.,
591 soot) in Arctic are one or two orders of magnitude smaller than observations (Wang et
592 al., 2011; Liu et al., 2012a).

593 For a more detailed comparison at warm temperature regions, spatial distributions
594 of model IN(10s) concentrations from the simulation PDF are shown in Figure 12
595 with some field measurements of IN concentrations around the globe (DeMott et al.
596 (2010), Central USA, $239\ \text{K} < T < 246\ \text{K}$ and $241\ \text{K} < T < 258\ \text{K}$; Rosinski et al.

597 (1987), Central Pacific, $254 \text{ K} < T < 260.5 \text{ K}$; Rosinski et al. (1995), East China Sea,
598 $T = 253 \text{ K}$; Bigg et al. (1973), South of Australia, $T = 258 \text{ K}$). In the East China Sea,
599 Brazil and Central USA regions, as there is only one single field campaign at each
600 region (i.e., only one single circle at each region in the Figure 12) and their colors are
601 similar as the background colors of modeled IN(10s) concentrations, we utilize
602 darkgreen rectangles to highlight them for seeing them clearly. The model IN(10s)
603 concentrations are selected for three specific temperatures which fall into the
604 corresponding range of observed temperatures as specified in each plot. All the field
605 measurements are located on surface, and thus we also use interstitial aerosol
606 concentrations at surface as input to diagnose IN concentrations. It can be seen that
607 the model IN(10s) concentrations are in agreement with observations, especially at
608 East China Sea, Brazil and Central USA. In near-surface-air over marine regions,
609 compared to dust IN, marine biogenic IN (types of marine biogenic particles include
610 marine microorganisms, exopolymer secretions/colloidal aggregates, glassy organic
611 aerosols, crystalline hydrated NaCl and frost flowers) are most likely to play a
612 dominant role in determining IN concentrations at high temperatures. Thus over the
613 Southern Ocean at 258 K , especially near the Antarctic coast, the model greatly
614 underestimates IN(10s) concentrations (Burrows et al., 2013). Another region where
615 the model significantly underestimates IN(10s) concentrations at 258 K is over the
616 Pacific. In the remote marine boundary layer of equatorial Pacific Ocean, due to ocean
617 upwelling, ship-based measurements found that atmospheric IN concentrations were
618 associated with high concentrations of biogenic materials (Rosinski et al., 1987).

619 Therefore, from Figures 11 and 12, the α -PDF model enhances the IN concentrations
620 at warm temperatures and agrees well with observations, which can be attributed to a
621 distribution of contact angles.

622 Georgii and Kleinjung (1967) found that IN number concentrations correlate well
623 with the number concentration of coarse mode aerosol particles but not with the total
624 aerosol number concentration, which is dominated by smaller particles. More recent
625 IN measurements with the CFDC obtained the similar results (DeMott et al., 2006;
626 DeMott et al., 2010; DeMott et al., 2014). Figure 13 shows the model IN(10s)
627 concentrations in the CNT and PDF simulations as a function of number
628 concentrations of aerosols with diameter larger than 0.5 μm (Na_{500}), sampling at $T =$
629 -21°C (Figure 13(a) and Figure 13(b)) which is the temperature used in the
630 observations (DeMott et al., 2006; Georgii and Kleinjung, 1967) and sampling at $T =$
631 -27°C (Figure 13(c) and Figure 13(d)) to compare with DeMott et al. (2014) with the
632 same processing temperature. In CAM5, we sample Na_{500} as follows: dust number
633 concentration in the accumulation mode with the diameter larger than 0.5 μm is
634 calculated with predicted dust mass mixing ratio in this mode and prescribed size
635 distribution for transported dust (Zender et al., 2003) (transported dust is in coarse
636 mode with mass median diameter 2.524 μm and standard deviation is 2.0). Dust
637 number concentration in the coarse mode is calculated from the predicted total
638 number concentration in the coarse mode weighted by the mass fraction of dust in this
639 mode. Then we use these two dust number concentration as the Na_{500} . We neglect the
640 contribution of soot (due to its smaller size) and sea salt to Na_{500} . In Figure 13(a) and

641 Figure 13(b), for both the CNT and PDF simulations, almost all dots locate
642 in-between the two power-law fits by DeMott et al. (2006) and Georgii and Kleinjung
643 (1967). Compared to the CNT simulation, the model IN(10s) concentrations simulated
644 from the PDF simulation shift a little upwards. In order to compare with DeMott et al.
645 (2014), we convert modeled Na_{500} and IN(10s) to those at standard temperature and
646 pressure conditions and the results are shown in Figure 13(c) and Figure 13(d). Both
647 in the CNT and PDF simulations, the magnitude of the model IN(10s) concentrations
648 are at and around the DeMott et al. (2014) proposed parameterization (solid red line),
649 thus yielding excellent agreement. The DeMott et al. (2014) parameterization,
650 developed from the DeMott et al. (2010) parameterization to account for additional
651 aerosol compositional dependencies, is for the dust ice nuclei exclusively. For
652 atmospheric application, an additional correction factor is introduced to account for
653 the underestimate of the immersion freezing fraction of mineral dust particles for
654 CFDC data. Their parameterization reflects the mineral dust data from the Saharan or
655 Asian regions very well and indicates they can be parameterized as a common particle
656 type for global modeling. Therefore, the atmospheric application of our
657 parameterization based on Saharan dust is successfully confirmed by DeMott et al.
658 (2014).

659

660 **4.6. Aerosol Indirect Effect**

661 Table 4 lists the global and annual mean cloud and radiative properties for the
662 present-day simulations and differences of these variables between the present-day

663 and preindustrial simulations. As for the present-day experiments, with the
664 implementation of two stochastic heterogeneous ice nucleation parameterizations, the
665 global mean ice water path (IWP) decreases for the CNT and all the PDF simulations
666 compared to the CTL simulation due to fewer nucleated ice crystals in the CNT and
667 PDF simulations. This can be confirmed from the comparison of the vertically
668 integrated column ice crystal number concentration (ICENUM) in mixed-phase
669 clouds ($-37\text{ }^{\circ}\text{C} < T < 0\text{ }^{\circ}\text{C}$) among different simulations. The CTL simulation has the
670 largest ICENUM in mixed-phase clouds, which is because Meyers' scheme
671 overestimates the nucleated ice number concentrations (DeMott et al., 2010). As a
672 consequence, the CNT and all the PDF simulations exhibit larger global mean liquid
673 water path (LWP) than that in the CTL simulation. This is because fewer ice crystals
674 slow down Wegener-Bergeron-Findeisen process, and thus increase the liquid water
675 content. The larger (smaller) mean contact angle with the smaller (larger) active
676 fraction in MU1 (MU2) in the PDF sensitivity simulations results in smaller (larger)
677 ICENUM in the mixed-phase clouds.

678 The LWP and IWP changes between present-day and pre-industry in the CTL
679 simulation are 3.26 g m^{-2} and 0.14 g m^{-2} respectively, while those in the CNT and
680 PDF simulations are much larger, especially the IWP change. There may be two
681 reasons that cause changes of IWP between the present-day and preindustrial
682 simulations with the new parameterizations to be generally larger than those in CTL.
683 One is increased dust concentrations (partly due to less efficient wet scavenging) and
684 increased soot concentrations in the PD simulations (the default scheme in CTL

685 doesn't link to aerosols). The other reason may be that soot is taken into account in
686 new parameterizations, which enlarges the differences between the present-day and
687 preindustrial simulations. Larger changes of IWP and LWP between present-day and
688 pre-industry in the CNT and PDF simulations lead to larger changes of shortwave
689 cloud forcing (SWCF) and longwave cloud forcing (LWCF). The SWCF change
690 differs by 0.18 W m^{-2} and LWCF change by 0.26 W m^{-2} between the CTL and CNT
691 simulations (0.30 W m^{-2} and 0.32 W m^{-2} between the CTL and PDF simulations
692 respectively), although the net cloud forcing change differs by less than 0.1 W m^{-2} .
693 The changes of total cloud cover (TCC), low-cloud cover (LCC) and integrated
694 column ice crystal number concentration (ICENUM) in the mixed-phase clouds
695 between present-day and pre-industry are also larger in the CNT and PDF simulations
696 than those in the CTL simulation.

697

698 **5. Conclusions**

699 A classical-nucleation-theory-based parameterization of heterogeneous ice
700 nucleation is implemented in CAM5 based on Hoose et al. (2010). In addition, we
701 make further improvements by introducing a probability distribution of contact angles
702 for the freezing process by natural dust. We fit the uncertain parameters of the
703 single- α and the α -PDF models to laboratory data for natural dust and BC (soot).
704 Compared to the single- α model, the α -PDF model has a better agreement with
705 observations at warm temperatures ($T > -20^\circ\text{C}$) by enhancing the IN number
706 concentrations and further results in weaker temperature dependence of IN number

707 concentration. Therefore, more ice crystals can form at low altitudes (with warm
708 temperatures) from the α -PDF model than those from the single- α model.

709 From the sensitivity tests with the α -PDF model, we find that though the change of
710 mean contact do not change the slope of variations of active fraction with temperature,
711 it still can change the active fraction at a given temperature. When increasing
712 (reducing) the mean contact angle, the active fraction will decrease (increase).
713 Meanwhile, the increase of standard deviation will lead to a transition of the
714 nucleation behavior: from stochastic behavior to singular behavior. Judged from the
715 absolute changes of the active fraction at a given temperature (not from its
716 temperature dependence), the mean contact angle has a larger impact on the active
717 fraction than that of standard deviation, which is consistent with the cloud-resolving
718 model results by Kulkarni et al. (2012). Immersion freezing by natural dust in both
719 single- α and α -PDF models is the dominant nucleation mechanism in mixed-phase
720 clouds, consistent with Hoose et al. (2010). After implementing the new
721 parameterizations, there are significant boosts to LWP due to effectively reducing the
722 nucleated ice number concentration. The new parameterizations also induce more
723 significant aerosol indirect effect than the default parameterization.

724 Although the heterogeneity of individual particles in the aerosol population has
725 been taken into account with introducing the α -PDF model, the heterogeneity on the
726 surface area of each particle can also influence the freezing behavior. Therefore, other
727 stochastic models considering the heterogeneity of surface area like the active site

728 model and the soccer ball model (Niedermeier et al., 2014) should be implemented
729 and then their behaviors should be explored in global models.

730

731 **Acknowledgment**

732 We would like to thank P. J. DeMott for providing the CFDC data shown in Fig. 10
733 and Fig. 11. This research was supported by the Office of Science of the US
734 Department of Energy (DOE) as part of the Earth System Modeling Program. We
735 would like to acknowledge the use of computational resources (ark:/85065/d7wd3xhc)
736 at the NCAR-Wyoming Supercomputing Center provided by the National Science
737 Foundation and the State of Wyoming, and supported by NCAR's Computational and
738 Information Systems Laboratory. CH acknowledges funding by the Helmholtz
739 Association through the President's Initiative and Networking Fund and by the
740 Deutsche Forschungsgemeinschaft through project FOR 1525. We would like to give
741 many thanks to the anonymous reviewers for their helpful suggestions.

742

743 **References**

744 Abdul-Razzak, H., and Ghan, S. J.: A parameterization of aerosol activation: 2.
745 Multiple aerosol types, *Journal of Geophysical Research: Atmospheres*, 105,
746 6837-6844, 10.1029/1999JD901161, 2000.

747

748 Ansmann, A., Tesche, M., Althausen, D., Müller, D., Seifert, P., Freudenthaler, V.,
749 Heese, B., Wiegner, M., Pisani, G., Knippertz, P., and Dubovik, O.: Influence of

750 Saharan dust on cloud glaciation in southern Morocco during the Saharan Mineral
751 Dust Experiment, *Journal of Geophysical Research: Atmospheres*, 113, D04210,
752 10.1029/2007JD008785, 2008.

753

754 Barahona, D.: On the ice nucleation spectrum, *Atmos. Chem. Phys.*, 12, 3733-3752,
755 10.5194/acp-12-3733-2012, 2012.

756

757 Bigg, E. K.: The formation of atmospheric ice crystals by the freezing of droplets,
758 *Quarterly Journal of the Royal Meteorological Society*, 79, 510-519,
759 10.1002/qj.49707934207, 1953.

760

761 Bigg, E. K.: Ice Nucleus Concentrations in Remote Areas, *Journal of the Atmospheric*
762 *Sciences*, 30, 1153-1157, 10.1175/1520-0469(1973)030<1153:INCIRA>2.0.CO;2,
763 1973.

764

765 Bretherton, C. S., and Park, S.: A New Moist Turbulence Parameterization in the
766 Community Atmosphere Model, *Journal of Climate*, 22, 3422-3448,
767 10.1175/2008JCLI2556.1, 2009.

768

769 Bunker, K. W., China, S., Mazzoleni, C., Kostinski, A., and Cantrell, W.:
770 Measurements of ice nucleation by mineral dusts in the contact mode, *Atmospheric*
771 *Chemistry and Physics Discussions*, 12, 20291-20309, 2012.

772

773 Burrows, S. M., Hoose, C., Pöschl, U., and Lawrence, M. G.: Ice nuclei in marine air:
774 biogenic particles or dust?, *Atmos. Chem. Phys.*, 13, 245-267,
775 10.5194/acp-13-245-2013, 2013.

776

777 Chen, J. P., Hazra, A., and Levin, Z.: Parameterizing ice nucleation rates using
778 contact angle and activation energy derived from laboratory data, *Atmos. Chem. Phys.*,
779 8, 7431-7449, 10.5194/acp-8-7431-2008, 2008.

780

781 Cooper, W. A.: A Possible Mechanism for Contact Nucleation, *Journal of the*
782 *Atmospheric Sciences*, 31, 1832-1837,
783 10.1175/1520-0469(1974)031<1832:APMFCN>2.0.CO;2, 1974.

784

785 de Boer, G., Morrison, H., Shupe, M. D., and Hildner, R.: Evidence of liquid
786 dependent ice nucleation in high-latitude stratiform clouds from surface remote
787 sensors, *Geophysical Research Letters*, 38, L01803, 10.1029/2010GL046016, 2011.

788

789 DeMott, P. J.: An Exploratory Study of Ice Nucleation by Soot Aerosols, *Journal of*
790 *Applied Meteorology*, 29, 1072-1079,
791 10.1175/1520-0450(1990)029<1072:AESOIN>2.0.CO;2, 1990.

792

793 DeMott, P. J., Cziczo, D. J., Prenni, A. J., Murphy, D. M., Kreidenweis, S. M.,
794 Thomson, D. S., Borys, R., and Rogers, D. C.: Measurements of the concentration and
795 composition of nuclei for cirrus formation, Proceedings of the National Academy of
796 Sciences, 100, 14655-14660, 10.1073/pnas.2532677100, 2003.

797

798 DeMott, P. J., Prenni, A. J., Richardson, M. S., Kreidenweis, S. M., Twohy, C. H.,
799 and Rogers D. C.: Ice nuclei variability, relation to ambient aerosol properties, and
800 impacts on mixed-phase clouds. Preprints, 12th Conf. on Cloud Physics, Madison, WI,
801 Amer. Meteor. Soc., 2.1, 10 July 2006 [Available online at
802 http://ams.confex.com/ams/Madison2006/techprogram/paper_113242.htm.]

803

804 DeMott, P. J., Prenni, A. J., Liu, X., Kreidenweis, S. M., Petters, M. D., Twohy, C. H.,
805 Richardson, M. S., Eidhammer, T., and Rogers, D. C.: Predicting global atmospheric
806 ice nuclei distributions and their impacts on climate, Proceedings of the National
807 Academy of Sciences, 107, 11217-11222, 10.1073/pnas.0910818107, 2010.

808

809 DeMott, P. J., Möhler, O., Stetzer, O., Vali, G., Levin, Z., Petters, M. D., Murakami,
810 M., Leisner, T., Bundke, U., Klein, H., Kanji, Z. A., Cotton, R., Jones, H., Benz, S.,
811 Brinkmann, M., Rzesanke, D., Saathoff, H., Nicolet, M., Saito, A., Nillius, B.,
812 Bingemer, H., Abbatt, J., Ardon, K., Ganor, E., Georgakopoulos, D. G., and Saunders,
813 C.: Resurgence in Ice Nuclei Measurement Research, Bulletin of the American
814 Meteorological Society, 92, 1623-1635, 10.1175/2011BAMS3119.1, 2011.

815

816 DeMott, P. J., Prenni, A. J., McMeeking, G. R., Sullivan, R. C., Petters, M. D., Tobo,
817 Y., Niemand, M., Möhler, O., Snider, J. R., Wang, Z., and Kreidenweis, S. M.:
818 Integrating laboratory and field data to quantify the immersion freezing ice nucleation
819 activity of mineral dust particles, *Atmos. Chem. Phys. Discuss.*, 14, 17359-17400,
820 10.5194/acpd-14-17359-2014, 2014.

821

822 Diehl, K., and Wurzler, S.: Heterogeneous Drop Freezing in the Immersion Mode:
823 Model Calculations Considering Soluble and Insoluble Particles in the Drops, *Journal*
824 *of the Atmospheric Sciences*, 61, 2063-2072,
825 10.1175/1520-0469(2004)061<2063:HDFITI>2.0.CO;2, 2004.

826

827 Ervens, B., and Feingold, G.: Sensitivities of immersion freezing: Reconciling classical
828 nucleation theory and deterministic expressions, *Geophysical Research Letters*, 40,
829 3320-3324, 10.1002/grl.50580, 2013.

830

831 Georgii, H., and Kleinjung, E.: Relations between the chemical composition of
832 atmospheric aerosol particles and the concentration of natural ice nuclei, *J. Rech.*
833 *Atmos*, 3, 145-156, 1967.

834

835 Gettelman, A., Morrison, H., and Ghan, S. J.: A New Two-Moment Bulk Stratiform
836 Cloud Microphysics Scheme in the Community Atmosphere Model, Version 3

837 (CAM3). Part II: Single-Column and Global Results, *Journal of Climate*, 21,
838 3660-3679, 10.1175/2008JCLI2116.1, 2008.

839

840 Gettelman, A., Liu, X., Ghan, S. J., Morrison, H., Park, S., Conley, A. J., Klein, S. A.,
841 Boyle, J., Mitchell, D. L., and Li, J. L. F.: Global simulations of ice nucleation and ice
842 supersaturation with an improved cloud scheme in the Community Atmosphere
843 Model, *Journal of Geophysical Research: Atmospheres*, 115, D18216,
844 10.1029/2009JD013797, 2010.

845

846 Hoose, C., Lohmann, U., Bennartz, R., Croft, B., and Lesins, G.: Global simulations
847 of aerosol processing in clouds, *Atmos. Chem. Phys.*, 8, 6939–6963, 2008a.

848

849 Hoose, C., Lohmann, U., Erdin, R., and Tegen, I.: The global influence of dust
850 mineralogical composition on heterogeneous ice nucleation in mixed-phase clouds,
851 *Environmental Research Letters*, 3, 025003, 2008b.

852

853 Hoose, C., Kristjánsson, J. E., Chen, J.-P., and Hazra, A.: A Classical-Theory-Based
854 Parameterization of Heterogeneous Ice Nucleation by Mineral Dust, Soot, and
855 Biological Particles in a Global Climate Model, *Journal of the Atmospheric Sciences*,
856 67, 2483-2503, 10.1175/2010JAS3425.1, 2010.

857

858 Hoose, C., and Möhler, O.: Heterogeneous ice nucleation on atmospheric aerosols: a
859 review of results from laboratory experiments, *Atmos. Chem. Phys.*, 12, 9817-9854,
860 10.5194/acp-12-9817-2012, 2012.

861

862 Iacono, M. J., Delamere, J. S., Mlawer, E. J., Shephard, M. W., Clough, S. A., and
863 Collins, W. D.: Radiative forcing by long-lived greenhouse gases: Calculations with
864 the AER radiative transfer models, *J. Geophys. Res.*, 113, D13103,
865 doi:10.1029/2008JD009944, 2008.

866

867 Knopf, D. A., and Koop, T.: Heterogeneous nucleation of ice on surrogates of mineral
868 dust, *Journal of Geophysical Research: Atmospheres*, 111, D12201,
869 10.1029/2005JD006894, 2006.

870

871 Koehler, K. A., Kreidenweis, S. M., DeMott, P. J., Petters, M. D., Prenni, A. J., and
872 Möhler, O.: Laboratory investigations of the impact of mineral dust aerosol on cold
873 cloud formation, *Atmos. Chem. Phys.*, 10, 11955-11968, 10.5194/acp-10-11955-2010,
874 2010.

875

876 Kulkarni, G., Fan, J., Comstock, J. M., Liu, X., and Ovchinnikov, M.: Laboratory
877 measurements and model sensitivity studies of dust deposition ice nucleation, *Atmos.*
878 *Chem. Phys.*, 12, 7295-7308, 10.5194/acp-12-7295-2012, 2012.

879

880 Langham, E., and Mason, B.: The heterogeneous and homogeneous nucleation of
881 supercooled water, *Proceedings of the Royal Society of London. Series A.*
882 *Mathematical and Physical Sciences*, 247, 493-504, 1958.

883

884 Liu, X., and Penner, J. E.: Ice nucleation parameterization for global models,
885 *Meteorologische Zeitschrift*, 14, 499-514, 10.1127/0941-2948/2005/0059, 2005.

886

887 Liu, X., Penner, J. E., Ghan, S. J., and Wang, M.: Inclusion of Ice Microphysics in the
888 NCAR Community Atmospheric Model Version 3 (CAM3), *Journal of Climate*, 20,
889 4526-4547, 10.1175/JCLI4264.1, 2007.

890

891 Liu, X., Easter, R. C., Ghan, S. J., Zaveri, R., Rasch, P., Shi, X., Lamarque, J. F.,
892 Gettelman, A., Morrison, H., Vitt, F., Conley, A., Park, S., Neale, R., Hannay, C.,
893 Ekman, A. M. L., Hess, P., Mahowald, N., Collins, W., Iacono, M. J., Bretherton, C.
894 S., Flanner, M. G., and Mitchell, D.: Toward a minimal representation of aerosols in
895 climate models: description and evaluation in the Community Atmosphere Model
896 CAM5, *Geosci. Model Dev.*, 5, 709-739, 10.5194/gmd-5-709-2012, 2012a.

897

898 Liu, X., Shi, X., Zhang, K., Jensen, E. J., Gettelman, A., Barahona, D., Nenes, A., and
899 Lawson, P.: Sensitivity studies of dust ice nuclei effect on cirrus clouds with the

900 Community Atmosphere Model CAM5, *Atmos. Chem. Phys.*, 12, 12061-12079,
901 10.5194/acp-12-12061-2012, 2012b.

902

903 Lohmann, U., and Diehl, K.: Sensitivity Studies of the Importance of Dust Ice Nuclei
904 for the Indirect Aerosol Effect on Stratiform Mixed-Phase Clouds, *Journal of the*
905 *Atmospheric Sciences*, 63, 968-982, 10.1175/JAS3662.1, 2006.

906

907 Linke, C., Möhler, O., Veres, A., Mohácsi, Á., Bozóki, Z., Szabó, G., and Schnaiter, M.:
908 Optical properties and mineralogical composition of different Saharan mineral dust samples:
909 a laboratory study, *Atmos. Chem. Phys.*, 6, 3315-3323, 10.5194/acp-6-3315-2006, 2006.

910

911 Lüönd, F., Stetzer, O., Welti, A., and Lohmann, U.: Experimental study on the ice
912 nucleation ability of size-selected kaolinite particles in the immersion mode, *Journal*
913 *of Geophysical Research: Atmospheres*, 115, D14201, 10.1029/2009JD012959, 2010.

914

915 Määttänen, A., Vehkamäki, H., Lauri, A., Merikallio, S., Kauhanen, J., Savijärvi, H.,
916 and Kulmala, M.: Nucleation studies in the Martian atmosphere, *Journal of*
917 *Geophysical Research: Planets*, 110, E02002, 10.1029/2004JE002308, 2005.

918

919 Marcolli, C., Gedamke, S., Peter, T., and Zobrist, B.: Efficiency of immersion mode
920 ice nucleation on surrogates of mineral dust, *Atmos. Chem. Phys.*, 7, 5081-5091,
921 10.5194/acp-7-5081-2007, 2007.

922

923 Meyers, M. P., DeMott, P. J., and Cotton, W. R.: New Primary Ice-Nucleation
924 Parameterizations in an Explicit Cloud Model, *Journal of Applied Meteorology*, 31,
925 708-721, 10.1175/1520-0450(1992)031<0708:NPINPI>2.0.CO;2, 1992.

926

927 Möhler, O., Büttner, S., Linke, C., Schnaiter, M., Saathoff, H., Stetzer, O., Wagner, R.,
928 Krämer, M., Mangold, A., Ebert, V., and Schurath, U.: Effect of sulfuric acid coating
929 on heterogeneous ice nucleation by soot aerosol particles, *Journal of Geophysical*
930 *Research: Atmospheres*, 110, D11210, 10.1029/2004JD005169, 2005.

931

932 Möhler, O., Field, P., Connolly, P., Benz, S., Saathoff, H., Schnaiter, M., Wagner, R.,
933 Cotton, R., Krämer, M., and Mangold, A.: Efficiency of the deposition mode ice
934 nucleation on mineral dust particles, *Atmospheric Chemistry and Physics*, 6,
935 3007-3021, 2006.

936

937 Möhler, O., Benz, S., Saathoff, H., Schnaiter, M., Wagner, R., Schneider, J., Walter,
938 S., Ebert, V., and Wagner, S.: The effect of organic coating on the heterogeneous ice
939 nucleation efficiency of mineral dust aerosols, *Environ. Res. Lett.*, 3, 025007,
940 doi:10.1088/1748-9326/3/2/025007, 2008.

941

942 Morrison, H., and Gettelman, A.: A New Two-Moment Bulk Stratiform Cloud
943 Microphysics Scheme in the Community Atmosphere Model, Version 3 (CAM3). Part

944 I: Description and Numerical Tests, *Journal of Climate*, 21, 3642-3659,
945 10.1175/2008JCLI2105.1, 2008.

946

947 Murray, B., O'Sullivan, D., Atkinson, J., and Webb, M.: Ice nucleation by particles
948 immersed in supercooled cloud droplets, *Chemical Society Reviews*, 41, 6519-6554,
949 2012.

950

951 Neale, R. B., Richter, J. H., and Jochum, M.: The impact of convection on ENSO:
952 From a delayed oscillator to a series of events, *Journal of climate*, 21, 5904-5924,
953 2008.

954

955 Niedermeier, D., Hartmann, S., Shaw, R. A., Covert, D., Mentel, T. F., Schneider, J.,
956 Poulain, L., Reitz, P., Spindler, C., Clauss, T., Kiselev, A., Hallbauer, E., Wex, H.,
957 Mildenerger, K., and Stratmann, F.: Heterogeneous freezing of droplets with
958 immersed mineral dust particles – measurements and parameterization, *Atmos. Chem.*
959 *Phys.*, 10, 3601-3614, 10.5194/acp-10-3601-2010, 2010.

960

961 Niedermeier, D., Shaw, R. A., Hartmann, S., Wex, H., Clauss, T., Voigtländer, J., and
962 Stratmann, F.: Heterogeneous ice nucleation: exploring the transition from stochastic
963 to singular freezing behavior, *Atmos. Chem. Phys.*, 11, 8767-8775,
964 10.5194/acp-11-8767-2011, 2011.

965

966 Niedermeier, D., Ervens, B., Clauss, T., Voigtländer, J., Wex, H., Hartmann, S., and
967 Stratmann, F.: A computationally efficient description of heterogeneous freezing: A
968 simplified version of the Soccer ball model, *Geophysical Research Letters*, 41(2),
969 736-741., 2014.

970

971 Niemand, M., Möhler, O., Vogel, B., Vogel, H., Hoose, C., Connolly, P., Klein, H.,
972 Bingemer, H., DeMott, P., Skrotzki, J., and Leisner, T.: A
973 Particle-Surface-Area-Based Parameterization of Immersion Freezing on Desert Dust
974 Particles, *Journal of the Atmospheric Sciences*, 69, 3077-3092,
975 10.1175/JAS-D-11-0249.1, 2012.

976

977 Park, S., and Bretherton, C. S.: The University of Washington Shallow Convection
978 and Moist Turbulence Schemes and Their Impact on Climate Simulations with the
979 Community Atmosphere Model, *Journal of Climate*, 22, 3449-3469,
980 10.1175/2008JCLI2557.1, 2009.

981

982 Phillips, V. T. J., DeMott, P. J., and Andronache, C.: An Empirical Parameterization
983 of Heterogeneous Ice Nucleation for Multiple Chemical Species of Aerosol, *Journal*
984 *of the Atmospheric Sciences*, 65, 2757-2783, 10.1175/2007JAS2546.1, 2008.

985

986 Phillips, V. T. J., Demott, P. J., Andronache, C., Pratt, K. A., Prather, K. A., Subramanian, R.,
987 and Twohy, C.: Improvements to an Empirical Parameterization of Heterogeneous Ice

988 Nucleation and Its Comparison with Observations, *Journal of the Atmospheric Sciences*, 70,
989 378-409, 10.1175/JAS-D-12-080.1, 2012.

990

991 Pitter, R. L., and Pruppacher, H. R.: A wind tunnel investigation of freezing of small
992 water drops falling at terminal velocity in air, *Quarterly Journal of the Royal*
993 *Meteorological Society*, 99, 540-550, 10.1002/qj.49709942111, 1973.

994

995 Prenni, A. J., DeMott, P. J., Kreidenweis, S. M., Harrington, J. Y., Avramov, A.,
996 Verlinde, J., Tjernström, M., Long, C. N., and Olsson, P. Q.: Can Ice-Nucleating
997 Aerosols Affect Arctic Seasonal Climate?, *Bulletin of the American Meteorological*
998 *Society*, 88, 541-550, 10.1175/BAMS-88-4-541, 2007.

999

1000 Pruppacher, H. R. and Klett, J. D.: *Microphysics of Clouds and Precipitation*,
1001 *Atmospheric and Oceanographic Sciences Library*, Kluwer Academic Publishers,
1002 Dordrecht, The Netherlands, 1997.

1003

1004 Richardson, M. S., DeMott, P. J., Kreidenweis, S. M., Cziczo, D. J., Dunlea, E. J.,
1005 Jimenez, J. L., Thomson, D. S., Ashbaugh, L. L., Borys, R. D., Westphal, D. L.,
1006 Casuccio, G. S., and Lersch, T. L.: Measurements of heterogeneous ice nuclei in the
1007 western United States in springtime and their relation to aerosol characteristics,
1008 *Journal of Geophysical Research: Atmospheres*, 112, D02209,
1009 10.1029/2006JD007500, 2007.

1010

1011 Rogers, D. C., DeMott, P. J., Kreidenweis, S. M., and Chen, Y.: A Continuous-Flow
1012 Diffusion Chamber for Airborne Measurements of Ice Nuclei, *Journal of Atmospheric*
1013 *and Oceanic Technology*, 18, 725-741,
1014 [10.1175/1520-0426\(2001\)018<0725:ACFDCF>2.0.CO;2](https://doi.org/10.1175/1520-0426(2001)018<0725:ACFDCF>2.0.CO;2), 2001.

1015

1016 Rosinski, J., Haagenson, P. L., Nagamoto, C. T., and Parungo, F.: Nature of
1017 ice-forming nuclei in marine air masses, *Journal of Aerosol Science*, 18, 291-309,
1018 [http://dx.doi.org/10.1016/0021-8502\(87\)90024-3](http://dx.doi.org/10.1016/0021-8502(87)90024-3), 1987.

1019

1020 Rosinski, J., Nagamoto, C. T., and Zhou, M. Y.: Ice-forming nuclei over the East
1021 China Sea, *Atmospheric Research*, 36, 95-105,
1022 [http://dx.doi.org/10.1016/0169-8095\(94\)00029-D](http://dx.doi.org/10.1016/0169-8095(94)00029-D), 1995.

1023

1024 Seland, Ø., Iversen, T., Kirkevåg, A., and Storelvmo, T.: Aerosol-climate interactions
1025 in the CAM-Oslo atmospheric GCM and investigation of associated basic
1026 shortcomings, *Tellus A*, 60, 459-491, [10.1111/j.1600-0870.2008.00318.x](https://doi.org/10.1111/j.1600-0870.2008.00318.x), 2008.

1027

1028 Sullivan, R. C., Petters, M. D., DeMott, P. J., Kreidenweis, S. M., Wex, H.,
1029 Niedermeier, D., Hartmann, S., Clauss, T., Stratmann, F., Reitz, P., Schneider, J., and
1030 Sierau, B.: Irreversible loss of ice nucleation active sites in mineral dust particles

1031 caused by sulphuric acid condensation, *Atmos. Chem. Phys.*, 10, 11471-11487,
1032 10.5194/acp-10-11471-2010, 2010.

1033

1034 Vali, G.: Nucleation terminology, *J. Aerosol Sci*, 16, 575-576, 1985.

1035

1036 Wang, M., Ghan, S., Ovchinnikov, M., Liu, X., Easter, R., Kassianov, E., Qian, Y.,
1037 and Morrison, H.: Aerosol indirect effects in a multi-scale aerosol-climate model
1038 PNNL-MMF, *Atmos. Chem. Phys.*, 11, 5431-5455, 10.5194/acp-11-5431-2011, 2011.

1039

1040 Welti, A., Lüönd, F., Kanji, Z. A., Stetzer, O., and Lohmann, U.: Time dependence of
1041 immersion freezing: an experimental study on size selected kaolinite particles, *Atmos.*
1042 *Chem. Phys.*, 12, 9893-9907, 10.5194/acp-12-9893-2012, 2012.

1043

1044 Wheeler, M., and Bertram, A.: Deposition nucleation on mineral dust particles: a case
1045 against classical nucleation theory with the assumption of a single contact angle,
1046 *Atmospheric Chemistry and Physics*, 12, 1189-1201, 2012.

1047

1048 Wiacek, A., and Peter, T.: On the availability of uncoated mineral dust ice nuclei in
1049 cold cloud regions, *Geophysical Research Letters*, 36, L17801,
1050 10.1029/2009GL039429, 2009.

1051

1052 Xie, S., Boyle, J., Klein, S. A., Liu, X., and Ghan, S.: Simulations of Arctic
1053 mixed-phase clouds in forecasts with CAM3 and AM2 for M-PACE, *Journal of*
1054 *Geophysical Research: Atmospheres*, 113, D04211, 10.1029/2007JD009225, 2008.

1055

1056 Xie, S., Liu, X., Zhao, C., and Zhang, Y.: Sensitivity of CAM5-Simulated Arctic
1057 Clouds and Radiation to Ice Nucleation Parameterization, *Journal of Climate*, 26,
1058 5981-5999, 10.1175/JCLI-D-12-00517.1, 2013.

1059

1060 Young, K. C.: The Role of Contact Nucleation in Ice Phase Initiation in Clouds,
1061 *Journal of the Atmospheric Sciences*, 31, 768-776,
1062 10.1175/1520-0469(1974)031<0768:TROCNI>2.0.CO;2, 1974.

1063

1064 Zender, C. S., Bian, H., and Newman, D.: Mineral Dust Entrainment and Deposition
1065 (DEAD) model: Description and 1990s dust climatology, *Journal of Geophysical*
1066 *Research: Atmospheres*, 108, 4416, 10.1029/2002JD002775, 2003.

1067

1068 Zhang, G. J., and McFarlane, N. A.: Sensitivity of climate simulations to the
1069 parameterization of cumulus convection in the Canadian Climate Centre general
1070 circulation model, *Atmosphere-Ocean*, 33, 407-446, 1995.

1071

1072 Zimmermann, F., Weinbruch, S., Schütz, L., Hofmann, H., Ebert, M., Kandler, K.
1073 and Worringer, A.: Ice nucleation properties of the most abundant mineral dust
1074 phases, *J. Geophys. Res.*, 113 (D23204), 8576, doi:10.1029/2008JD010655, 2008.
1075
1076 Zobrist, B., Koop, T., Luo, B. P., Marcolli, C., and Peter, T.: Heterogeneous Ice
1077 Nucleation Rate Coefficient of Water Droplets Coated by a Nonadecanol Monolayer,
1078 *The Journal of Physical Chemistry C*, 111, 2149-2155, 10.1021/jp066080w, 2007.
1079

1080 **Tables**

1081 **Table 1.** Parameters for the ice nucleation parameterization in single contact angle (α) model. In the table, DeMott et al. (2011) and Koehler et
 1082 al. (2010) are Saharan Dust. $\Delta g^\#$ is the activation energy; $f_{i,max,x}$ is the maximum ice nucleating fraction.

1083

Aerosol	Reference	Nucleation mode	α ($^\circ$)	$\Delta g^\#$ (10^{-20} J)	$f_{i,max,x}$
Soot	DeMott (1990)	Immersion	48.0	14.15	0.01
Dust	DeMott et al. (2011)	Immersion	46.0	14.75	1
Soot	Möhler et al. (2005)	Deposition	28.0	-20	0.01
Dust	Koehler et al. (2010)	Deposition	20.0	-0.81	1

1084

1085

1086

1087 **Table 2.** Fit parameters obtained for the two models for the immersion freezing by dust. The root mean square errors (RMSE) between the fit
 1088 curves and the data are given. In the table, μ is the mean contact angle; σ is the standard deviation.

Model	Parameter/RMSE	CSU106	CSU108	ZINC106	ZINC108	ZINC110
Single- α	α ($^{\circ}$)	46.0	47.0	61.0	61.0	59.0
	$\Delta g^{\#}$ (10^{-20} J)	14.75	14.4	13.5	13.45	13.65
	RMSE	0.029	0.236	0.087	0.0983	0.147
α -PDF	μ ($^{\circ}$)	46.0	47.0	62.0	61.0	59.0
	σ	0.01	0.01	0.04	0.01	0.02
	RMSE	0.01	0.225	0.08	0.07	0.08

1089

1090 **Table 3.** Simulation descriptions

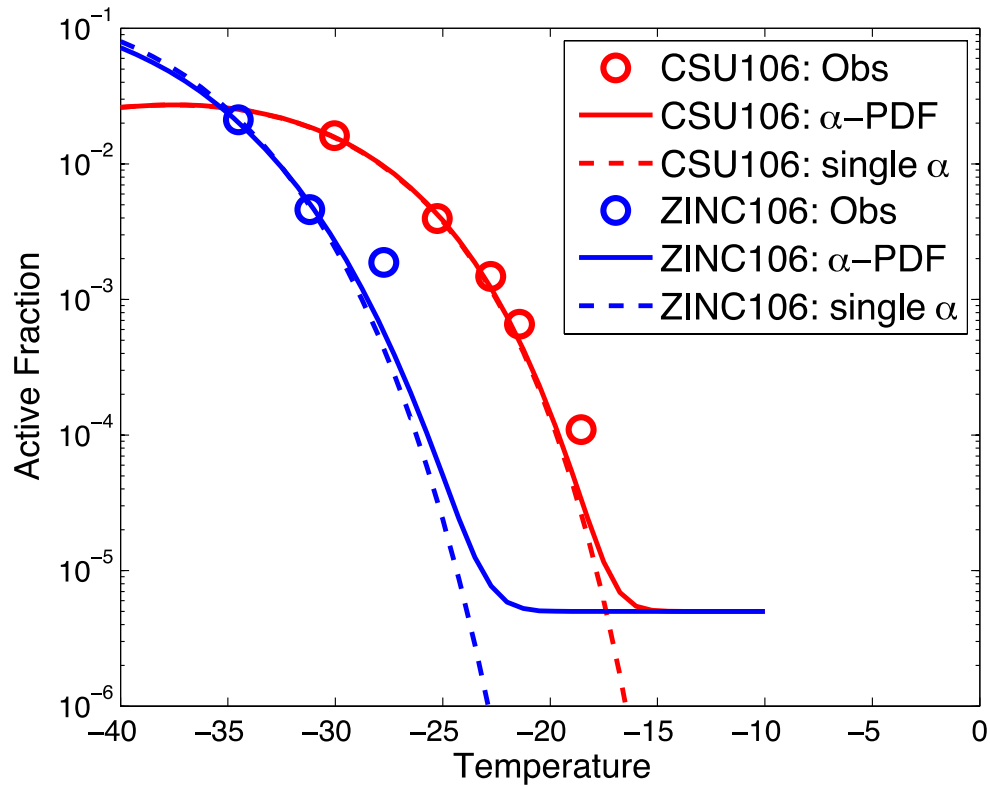
Simulation	Description
CTL	CAM5 with the default heterogeneous ice nucleation parameterization (Meyers et al. 1992)
CNT	As in CTL, but with the classical nucleation theory based on Hoose et al. (2010), using new fitting parameters in Table 1 (e.g., for immersion freezing on dust: $\alpha=46^\circ$, $\Delta g^\#(10^{-20} \text{ J})=14.75$)
PDF	As in CTL, but with the improved CNT by introducing α -PDF model in immersion freezing on dust ($\mu=46^\circ$, $\sigma=0.01$)
MU1	As in PDF, but with $\mu=31^\circ$, $\sigma=0.01$
MU2	As in PDF, but with $\mu=61^\circ$, $\sigma=0.01$
SD1	As in PDF but with $\mu=46^\circ$, $\sigma=0.04$ (4σ)
SD2	As in PDF but with $\mu=46^\circ$, $\sigma=0.08$ (8σ)

1091

1092 **Table 4.** Global annual mean fields for the present-day simulations and differences of these variables between present-day and preindustrial
1093 simulations. Variables listed in the table are: total cloud cover (TCC, %), low cloud cover (LCC, %), liquid water path (LWP, g m⁻²), ice water
1094 path (IWP, g m⁻²), shortwave cloud forcing (SWCF, W m⁻²), longwave cloud forcing (LWCF, W m⁻²) and integrated column ice number
1095 concentration in mixed-phase clouds (ICNUM, 10³cm⁻²)

Run	CTL	CNT	PDF	MU1	MU2	SD1	SD2
TCC	64.0	64.0	63.9	64.0	64.1	64.0	64.0
Δ TCC	0.14	0.42	0.28	0.57	0.59	0.44	0.62
LCC	43.6	43.1	43.1	43.1	43.2	43.1	43.1
Δ LCC	0.32	0.58	0.49	0.68	0.72	0.66	0.72
LWP	44.59	46.41	46.51	46.34	46.72	46.60	46.56
Δ LWP	3.26	3.66	3.80	3.73	3.98	3.96	3.77
IWP	17.78	16.10	16.22	16.28	16.23	16.27	16.24
Δ IWP	0.14	0.16	0.32	0.42	0.34	0.36	0.33
SWCF	-52.00	-52.10	-52.20	-52.17	-52.34	-52.24	-52.25
Δ SWCF	-1.64	-1.82	-1.94	-2.01	-2.08	-2.03	-2.05
LWCF	24.04	23.61	23.65	23.65	23.75	23.69	23.68
Δ LWCF	0.50	0.76	0.82	0.92	0.92	0.81	0.84
CF	-27.96	-28.47	-28.55	-28.52	-28.58	-28.55	-28.56
Δ CF	-1.14	-1.06	-1.13	-1.10	-1.16	-1.22	-1.21
ICNUM	2.863	2.366	2.395	2.407	2.381	2.401	2.389
Δ ICNUM	0.036	0.045	0.074	0.068	0.052	0.069	0.066

1096



1097

1098

1099 Figure 1. Active fractions determined with CSU106 and ZINC106 respectively
 1100 (DeMott et al., 2011) are presented as a function of temperature T (indicated by the
 1101 different color cycles). The different lines represent the single- α model and the
 1102 α -PDF model results fitting the experimentally determined active fractions
 1103 (parameters in two models are given in the Table 2).

1104
1105
1106
1107
1108
1109
1110
1111
1112
1113
1114
1115
1116
1117
1118
1119
1120

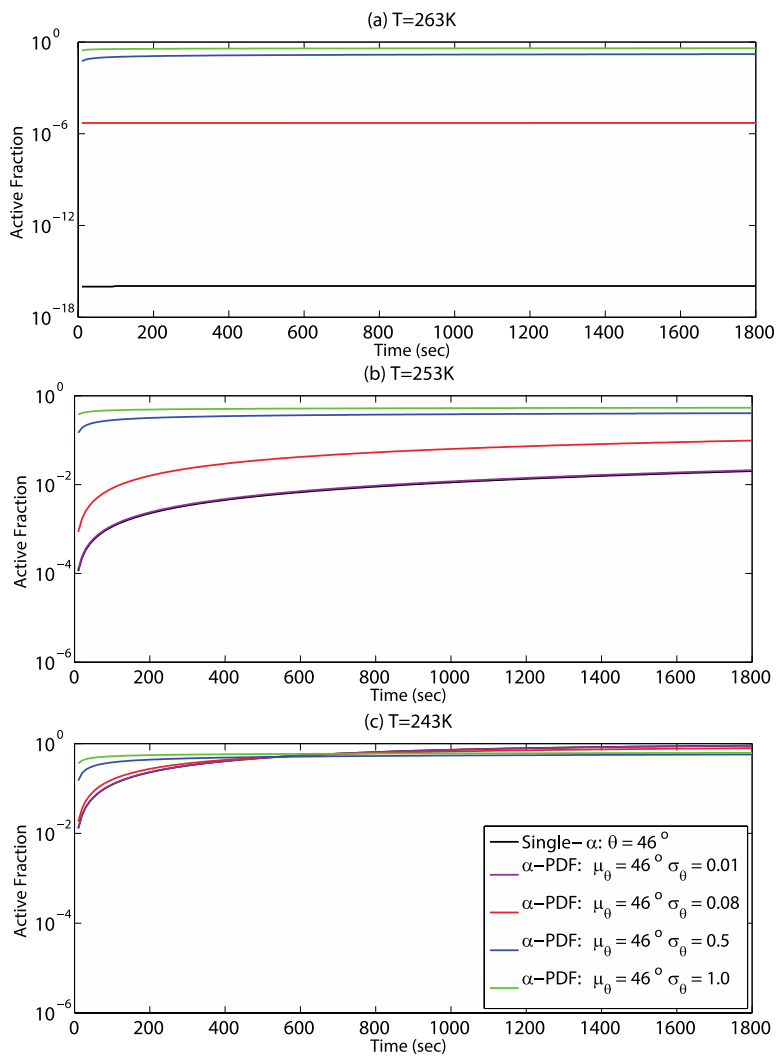


Figure 2. Calculated change in the active fraction with time at different temperatures for 300nm monodisperse particles and for different contact angle distributions.

1121

1122

1123

1124

1125

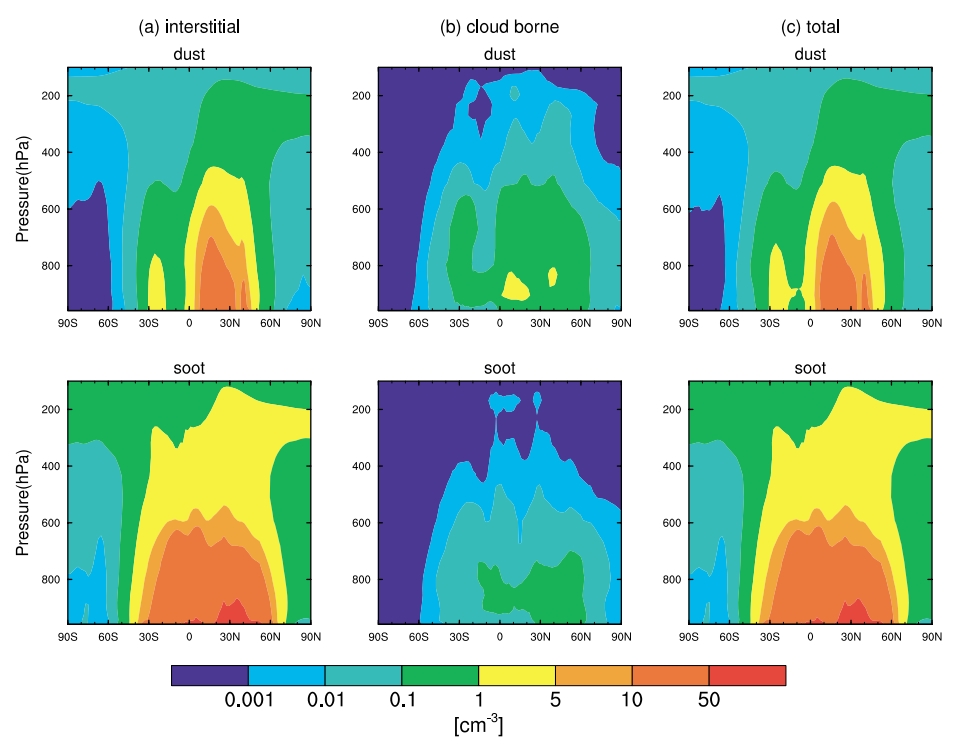
1126

1127

1128

1129

1130



1131 Figure 3. Zonal and annual mean number concentrations (cm^{-3}) of (a) interstitial, (b)

1132 cloud borne and (c) total mineral dust (upper) and soot particles (lower).

1133

1134
1135
1136
1137
1138
1139
1140
1141
1142
1143
1144
1145
1146

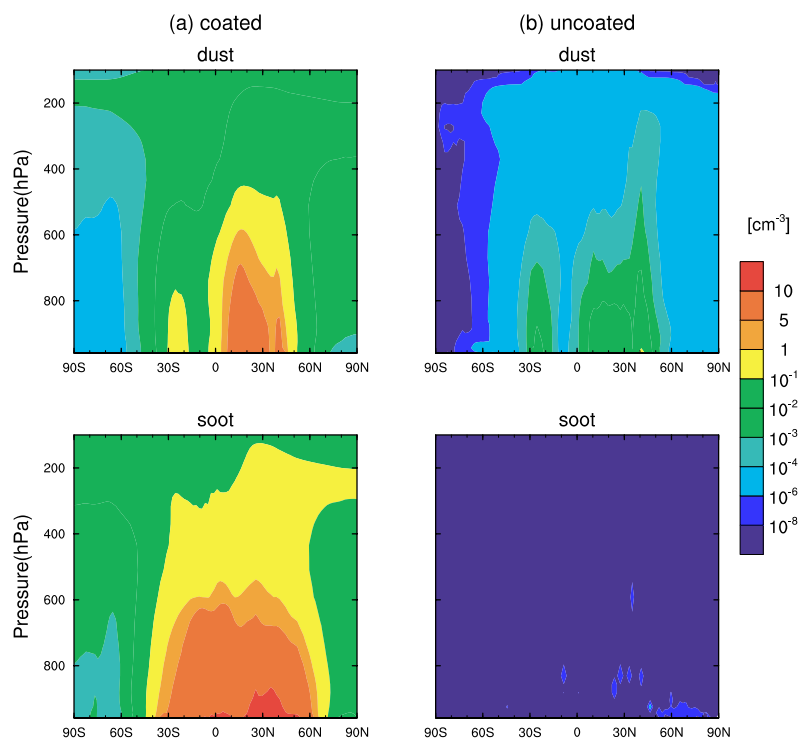
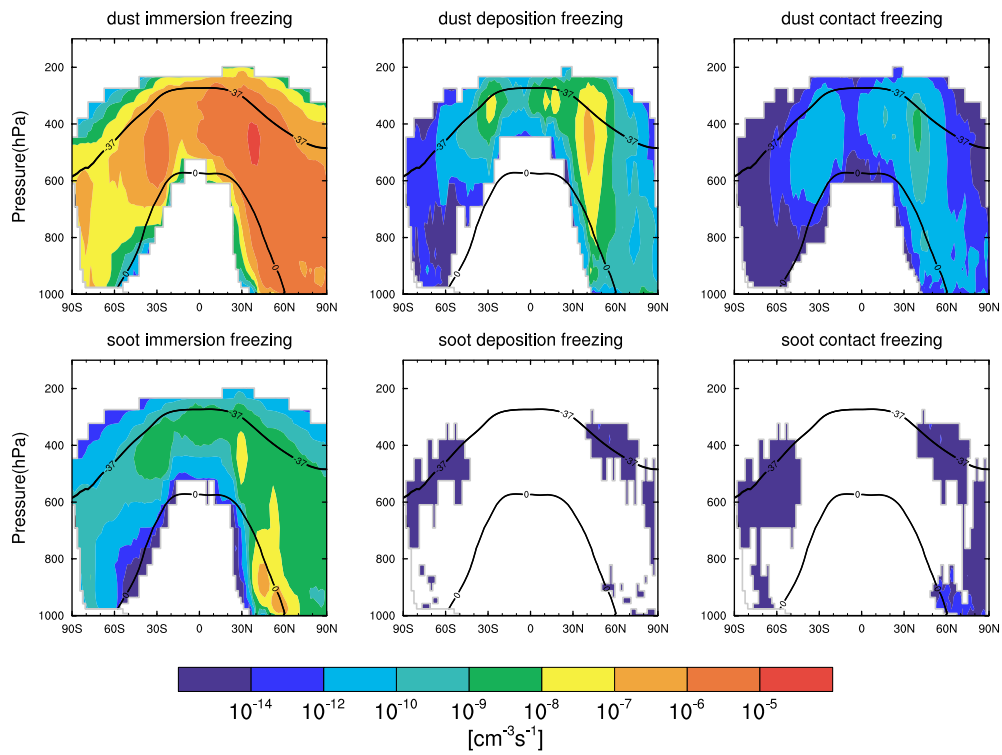


Figure 4. Zonal and annual mean number concentrations of (a) interstitial coated and (b) interstitial uncoated mineral dust (upper) and soot particles (lower).

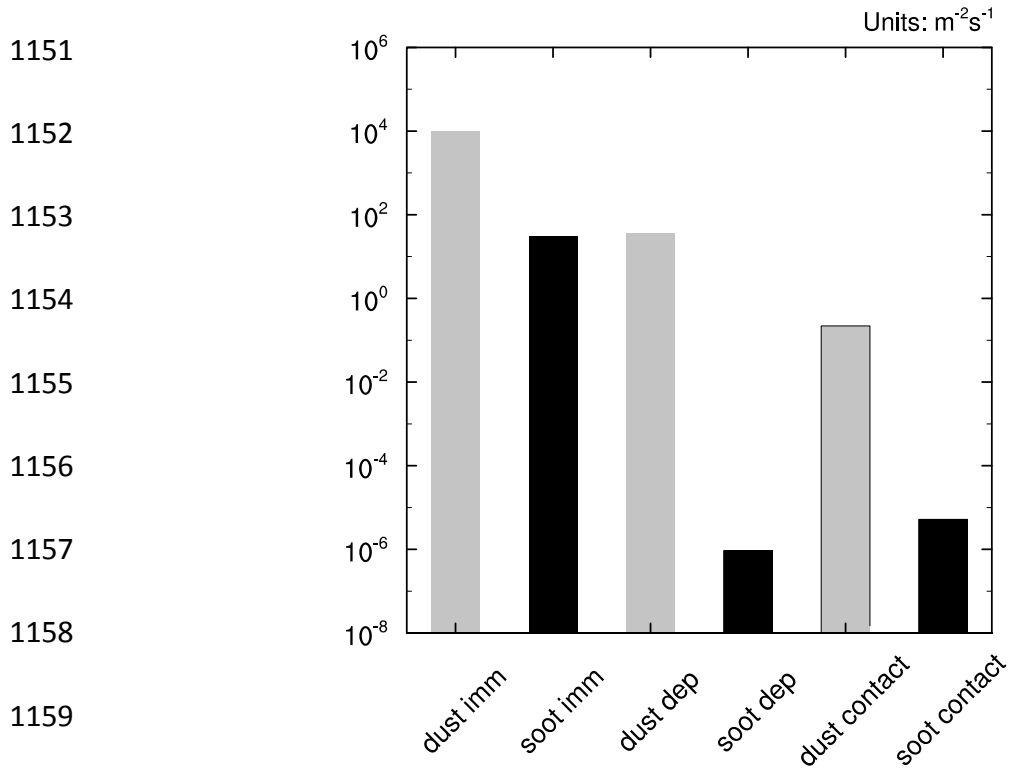


1147

1148

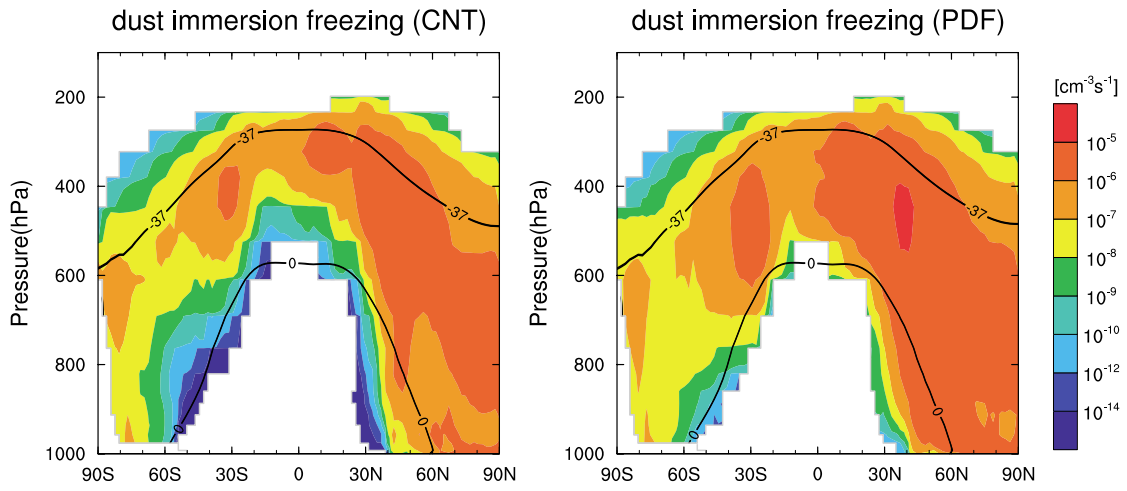
1149 Figure 5. Zonal and annual mean immersion, deposition, and contact freezing rates

1150 in the PDF simulation. Isotherms of 0 °C and -37 °C are plotted.



1161 Figure 6. Global and annual mean vertically integrated nucleation rates in the PDF
 1162 simulation.

1163



1164

1165

1166 Figure 7. Zonal and annual mean immersion freezing rates in the CNT and PDF

1167 simulations. Isotherms of 0°C and -37°C are plotted.

1168
 1169
 1170
 1171
 1172
 1173
 1174
 1175
 1176
 1177
 1178
 1179
 1180
 1181

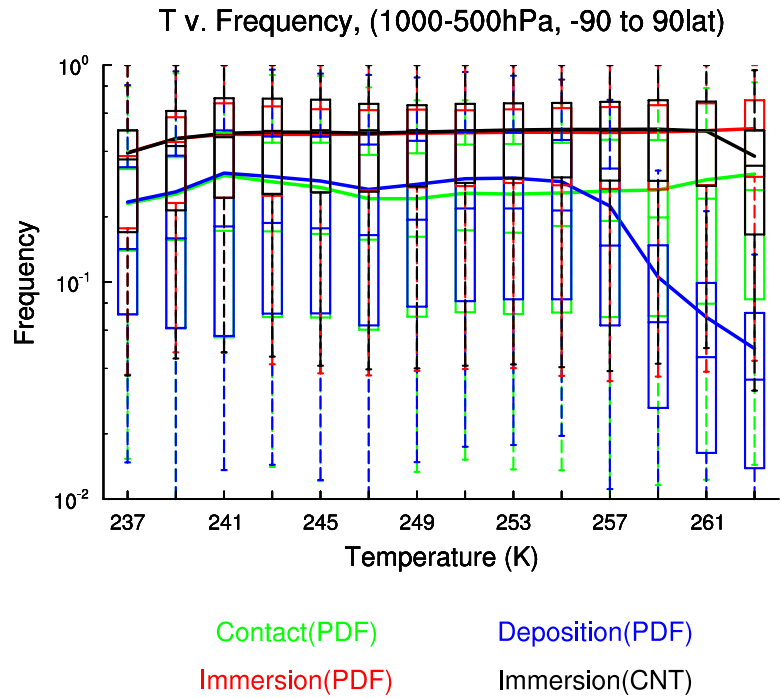
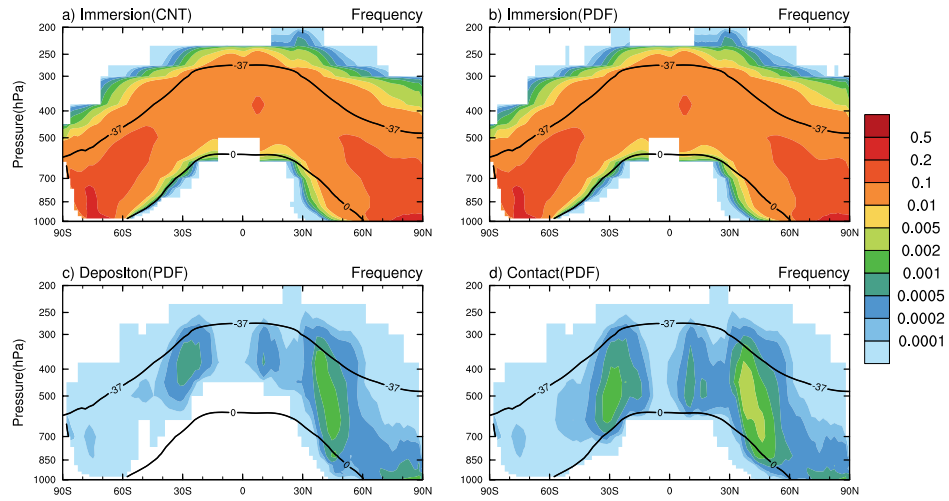


Figure 8. Simulated frequency of immersion freezing (red), deposition nucleation (blue) and contact nucleation (green) in the PDF simulation, and immersion freezing (black) in the CNT simulation as a function of temperature sampled every 3 hours. The whiskers represent the 5th and 95th percentiles and the boxes represent the 25th and 75th percentiles and the median.

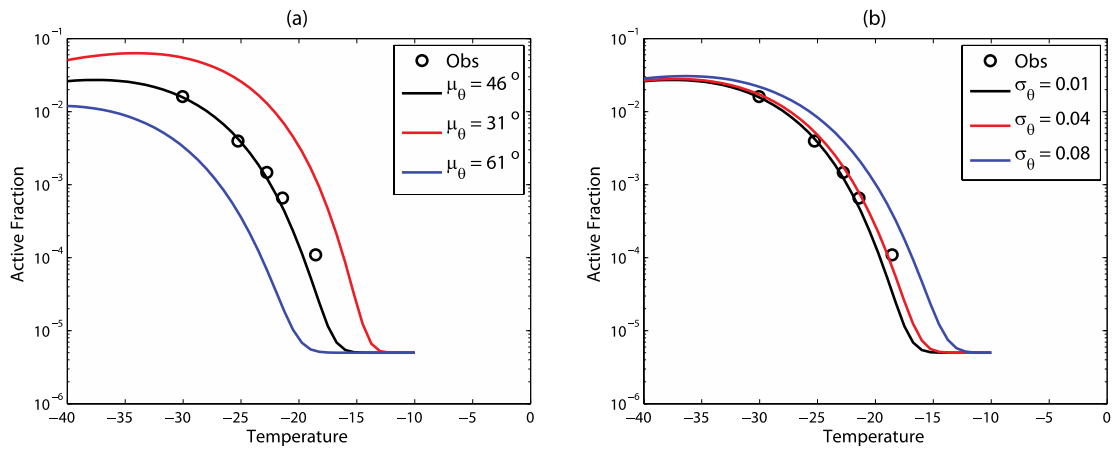
1182

1183



1184 Figure 9. Zonal and annual mean distribution of occurrence frequency of (a)
1185 immersion mode in the CNT simulation, and of (b) immersion, (c) deposition, and (d)
1186 contact freezing modes in the PDF simulation. Isotherms of 0 °C and -37 °C are
1187 plotted.

1188



1189

1190

1191 Figure 10. Active fraction as a function of temperature for the α -PDF model settings.

1192 Observation data is from CSU106 and the black solid line is its fit curve. The red

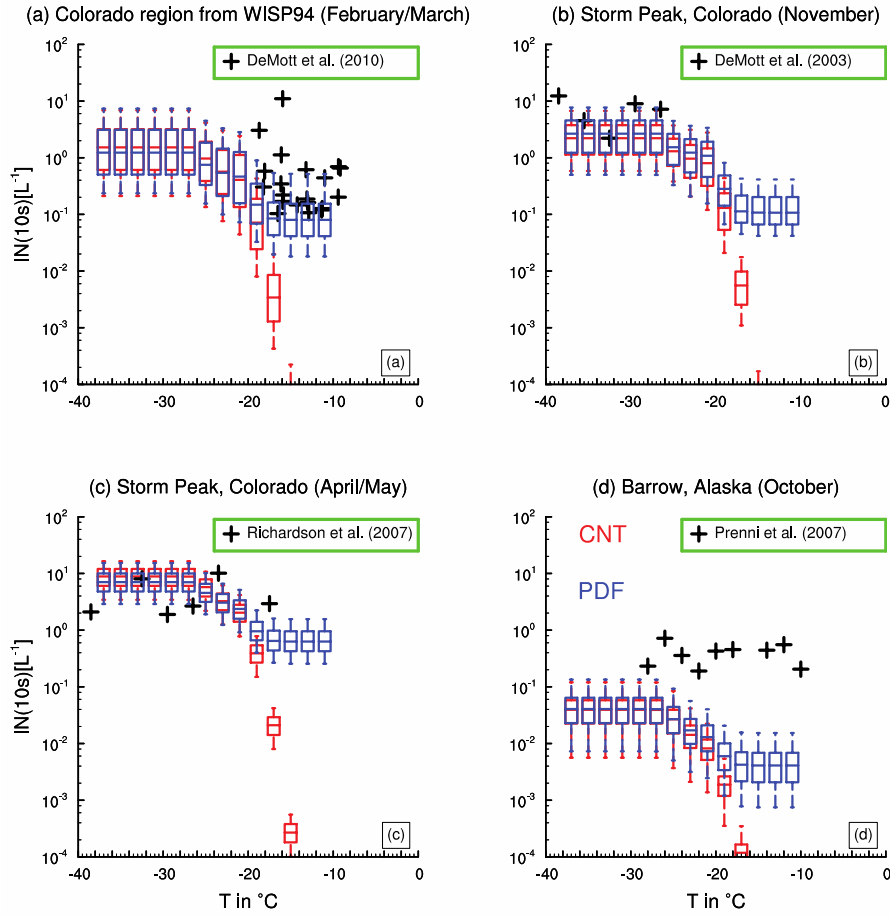
1193 and blue solid lines are sensitivity tests to (a) mean contact angle, and (b) standard

1194 deviation.

1195

1196

1197



1198 Figure 11. IN(10s) concentrations for specified temperature, selected at the grid

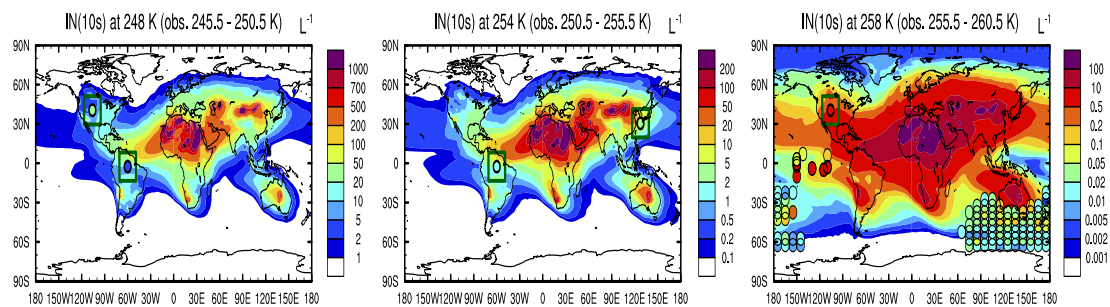
1199 points including the measurement locations and at the same pressure level as field

1200 observations in the CNT simulation (red boxes and whiskers) and in the PDF

1201 simulation (blue boxes and whiskers). The whiskers represent the 5th and 95th

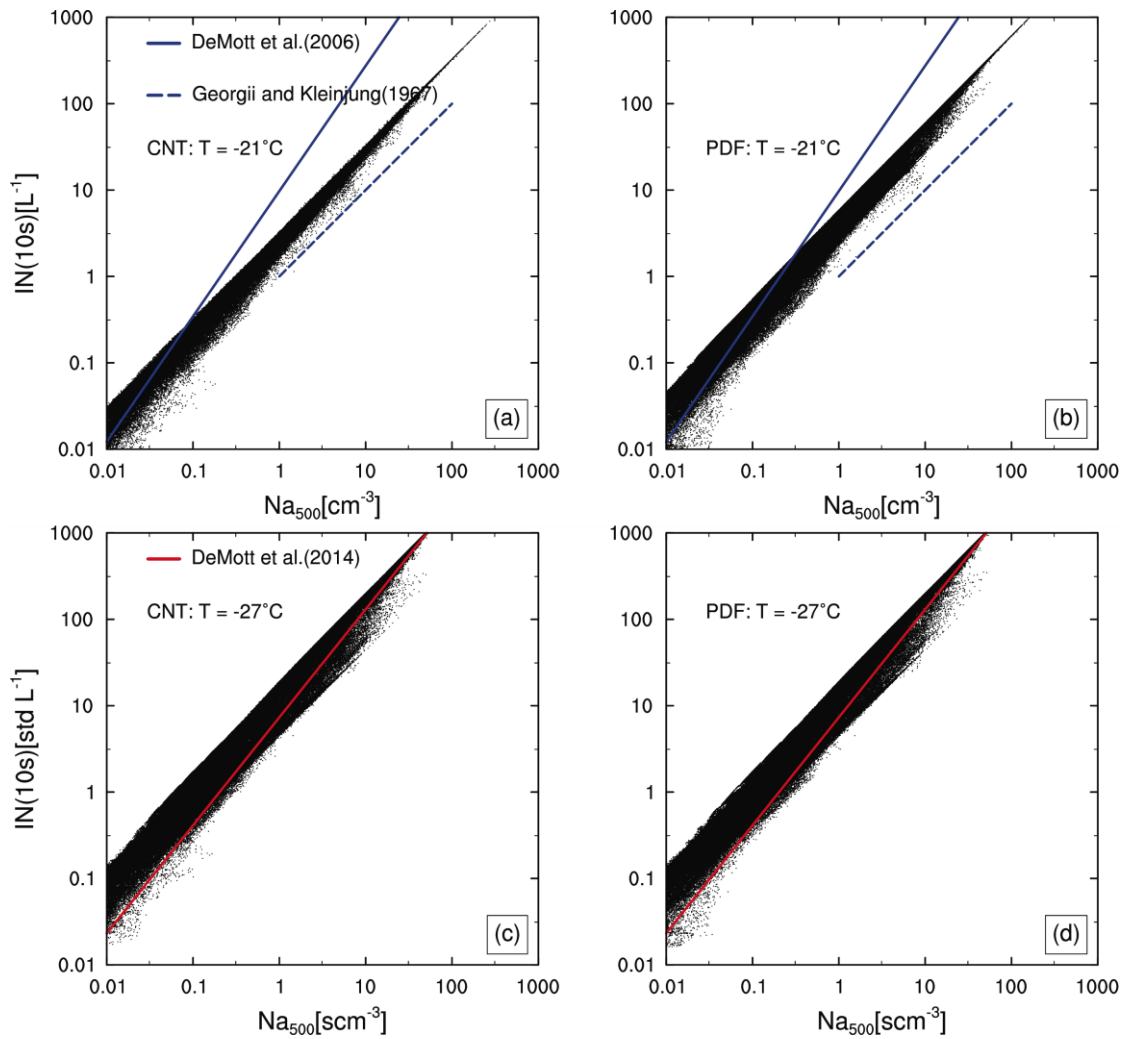
1202 percentiles, and the boxes represent the 25th and 75th percentiles and the median.

1203 The symbols indicate CFDC IN measurements.



1204

1205 Figure 12. Spatial comparison of IN(10s) concentration with field data. IN(10s)
 1206 concentrations are sampled for three specific temperatures which fall into the same
 1207 range of observed temperatures as chosen for measurements on the surface. The
 1208 field IN measurements are indicated by colored circles (DeMott et al. (2010) in
 1209 Central USA; Rosinski et al. (1987) in Central Pacific; Rosinski et al. (1995) in East
 1210 China Sea; Bigg et al. (1973) in South of Australia). Especially, field IN
 1211 measurements at East China Sea, Brazil and Central USA are highlighted by
 1212 darkgreen rectangles to see clearly.



1213

1214

1215 Figure 13. IN(10s) concentrations in the CNT and PDF simulations, displayed as a

1216 function of the number concentrations of aerosol particles with $d > 0.5 \mu\text{m}$ at (a and b)

1217 $T = -21^\circ\text{C}$ which is the observed temperature used in the power-law fit to observations

1218 (DeMott et al. 2006 (blue solid line); Georgii and Kleinjung 1967 (blue dash line))

1219 and at (c and d) $T = -27^\circ\text{C}$ which is used for the DeMott et al. (2014) proposed

1220 parameterization (solid red line)

1221

List of Figure Captions

<p>Figure 1</p>	<p>Active fractions determined with CSU106 and ZINC106 respectively (DeMott et al., 2011) are presented as a function of temperature T (indicated by the different color cycles). The different lines represent the single-α model and the α-PDF model results fitting the experimentally determined active fractions (parameters in two models are given in the Table 2).</p>
<p>Figure 2</p>	<p>Calculated change in the active fraction with time at different temperatures for 300nm monodisperse particles and for different contact angle distributions.</p>
<p>Figure 3</p>	<p>Zonal and annual mean number concentrations (cm^{-3}) of (a) interstitial, (b) cloud borne and (c) total mineral dust (upper) and soot particles (lower).</p>
<p>Figure 4</p>	<p>Zonal and annual mean number concentrations of (a) interstitial coated</p>

	and (b) interstitial uncoated mineral dust (upper) and soot particles (lower).
Figure 5	Zonal and annual mean immersion, deposition, and contact freezing rates in the PDF simulation. Isotherms of 0 °C and -37 °C are plotted.
Figure 6	Global and annual mean vertically integrated nucleation rates in the PDF simulation.
Figure 7	Zonal and annual mean immersion freezing rates in the CNT and PDF simulations. Isotherms of 0 °C and -37 °C are plotted.
Figure 8	Simulated frequency of immersion freezing (red), deposition nucleation (blue) and contact nucleation (green) in the PDF simulation, and immersion freezing (black) in the CNT simulation as a function of temperature sampled every 3 hours. The whiskers represent the 5th and 95th percentiles and the boxes represent the 25th and 75th percentiles

	and the median.
Figure 9	Zonal and annual mean distribution of occurrence frequency of (a) immersion mode in the CNT simulation, and of (b) immersion, (c) deposition, and (d) contact freezing modes in the PDF simulation. Isotherms of 0 °C and -37 °C are plotted.
Figure 10	Active fraction as a function of temperature for the α -PDF model settings. Observation data is from CSU106 and the black solid line is its fit curve. The red and blue solid lines are sensitivity tests to (a) mean contact angle, and (b) standard deviation.
Figure 11	IN(10s) concentrations for specified temperature, selected at the grid points including the measurement locations and at the same pressure level as field observations in the CNT simulation (red boxes and whiskers) and in the PDF simulation (blue boxes and whiskers). The whiskers represent the 5th and 95th

	<p>percentiles, and the boxes represent the 25th and 75th percentiles and the median</p> <p>The symbols indicate CFDC IN measurements..</p>
<p>Figure 12</p>	<p>Spatial comparison of IN(10s) concentration with field data. IN(10s) concentrations are sampled for three specific temperatures which fall into the same range of observed temperatures as chosen for measurements on the surface.</p> <p>The field IN measurements are indicated by colored circles (DeMott et al. (2010) in Central USA; Rosinski et al. (1987) in Central Pacific; Rosinski et al. (1995) in East China Sea; Bigg et al. (1973) in South of Australia). Especially, field IN measurements at East China Sea, Brazil and Central USA are highlighted by darkgreen rectangles to see clearly.</p>
<p>Figure 13</p>	<p>IN(10s) concentrations in the CNT and PDF simulations, displayed as a function of the number concentrations of aerosol</p>

	<p>particles with $d > 0.5 \mu\text{m}$ at (a and b) $T = -21^\circ\text{C}$ which is the observed temperature used in the power-law fit to observations (DeMott et al. 2006 (blue solid line); Georgii and Kleinjung 1967 (blue dash line)) and at (c and d) $T = -27^\circ\text{C}$ which is used for the DeMott et al. (2014) proposed parameterization (solid red line)</p>
--	---

1222

List of Table Captions	
Table 1	Parameters for the ice nucleation parameterization in single contact angle (α) model. In the table, DeMott et al. (2011) and Koehler et al. (2010) are Saharan Dust. $\Delta g^\#$ is the activation energy; $f_{i,max,x}$ is the maximum ice nucleating fraction.
Table 2	Fit parameters obtained for the two models for the immersion freezing by dust. The root mean square errors (RMSE) between the fit curves and the data are given. In the table, μ is the mean contact angle; σ is the standard deviation.
Table 3	Simulation descriptions
Table 4	Global annual mean fields for the present-day simulations and differences of these variables between present-day and preindustrial simulations. Variables listed in the table are: total cloud cover (TCC, %), low cloud cover (LCC, %), liquid water path (LWP, g m^{-2}), ice water

	path (IWP, g m^{-2}), shortwave cloud forcing (SWCF, W m^{-2}), longwave cloud forcing (LWCF, W m^{-2}) and integrated column ice number concentration in mixed-phase clouds (ICNUM, 10^3cm^{-2})
--	--

1223